Journal of Computational Physics **162,** 338–371 (2000)
doi:10.1006/jcph.2000.6538, available online at http://www.idealibrary.com on IDEAL®

Development of High-Order Taylor–Galerkin Schemes for LES

Olivier Colin[1]

Aerospatiale Matra Missiles/CERFACS, 42 Avenue Coriolis, 31057 Toulouse Cedex 01, France

and

Michael Rudgyard

Oxford University Computing Laboratory, Wolfson Building, Parks Road, Oxford OX1 3QD, United Kingdom
E-mail: Mike.Rudgyard@comlab.ox.ac.uk

Received June 15, 1999; revised April 6, 2000

In this paper we describe the implementation and development of a new Taylor–Galerkin finite-element scheme within an unstructured/hybrid, parallel solver. The scheme has been specifically conceived for unsteady LES: it is third-order in space and time and has a low dissipative error. Minimal additional CPU costs are achieved by using a new approximation of the finite-element integrals and a simple iterative method for the approximate inversion of the modified mass matrix. Basic convective tests are carried out in 2 and 3 dimensions for arbitrary elements. Numerical estimates of the order of convergence are presented on regular and perturbed grids. Finally, test cases that are relevant to LES are carried out, and these clearly demonstrate the important improvements that our new scheme offers relative to a selection of existing methods.

Key Words: Taylor–Galerkin methods; high-order schemes; convection; LES.

1. INTRODUCTION

For large eddy simulations of turbulence (LES), the quality of a computation is known to be as dependent on the accuracy of the numerical scheme and the computational mesh as on the LES model itself [1]. A poor mesh resolution and the use of a low-order scheme can contribute dramatically to the dissipation of eddies (through numerical dissipation errors) and to the distortion of their form (through numerical dispersion errors). For complex geometries, when unstructured or structured multi-block grids are required, the simplest and

[1] Present address: IFP, 1à 4 av. du Bois, Préau, 92852 Rueil-Malmaison, France. E-mail: Olivier.COLIN@ifp.fr.

0021-9991/00 $35.00

most common way to achieve the required level of accuracy is to use a relatively low-order finite-volume or finite-element scheme with a very fine mesh (see, e.g., [2]). Although the results of such computations may be impressive, the approach can be extremely costly.

This requirement for accuracy leads us to consider high-order methods, since the total cost of a calculation is likely to be lower if we increase the order of the numerical scheme rather than increasing the number of mesh points used. Indeed, the argument becomes even more convincing for three-dimensional problems. In practice, however, we need to ensure that the computational overhead generated by the high-order scheme is reasonably low. High-order spectral [3] or finite-difference [4] methods for structured grids have been successful for simple geometries because the overhead is small compared to the gain in accuracy. Related schemes have been generalized to unstructured meshes (e.g., [5]), but they become much more expensive due to the high-order quadrature that is needed and/or the increased CPU overheads associated with the larger stencils required.

For convection problems, third- or fourth-order Galerkin/Runge–Kutta finite-element schemes that use linear elements and Runge–Kutta time-stepping may easily be derived (we denote these as G/RK3 and G/RK4, respectively). Despite their simple formulation, these schemes suffer from some important shortcomings, namely that their accuracy drops dramatically on distorted meshes, and they do not dissipate node-to-node oscillations which may lead to spurious wave packets and cause instabilities on highly irregular meshes [6]. To some extent, both problems may be alleviated using an artificial viscosity method [7], although the definition of suitable models is not straightforward, and those used in the literature are often too dissipative for unsteady applications.

Of all of the finite-element schemes [8], the Taylor–Galerkin (TG) family seems to be one of the best candidates for obtaining third (or higher) order at a reasonable cost, as well as being suitable for nonlinear problems in higher space dimensions. Such schemes are generally less dissipative than common implementations of SUPG/Petrov–Galerkin or least-square schemes. Taylor–Galerkin schemes were originally derived by Donea [9] and have been extensively used for CFD computations over the last two decades. Donea [9] performed third- and fourth-order temporal Taylor expansions within the Galerkin formulation that led to a one-step third-order scheme called Euler–Taylor–Galerkin (ETG). This scheme was generalized to two-step schemes of third- and fourth-order (TTG3, TTG4A, TTG4B) by Quartapelle and Selmin [10]. Unlike the G/RK3 scheme, all of these schemes exhibit leading order dissipative terms which naturally damp node-to-node oscillations. However, they are more dissipative than G/RK3 across the whole frequency spectrum. Recent work by Oden *et al.* [11, 12] has demonstrated how Taylor–Galerkin schemes of order "2s" may be defined using "s" stages to achieve unconditional stability. Although these schemes may prove to be useful, they are not considered here because of the complexity and the cost involved in using adaptative hp-finite-elements.

In the present paper we shall describe a third-order Taylor–Galerkin approach for convective terms, that is both simple, effective, and, most importantly, well-suited for LES. The basic idea of LES is to resolve large-scale turbulent structures, which are dynamically more important, and then to simulate the action of scales smaller than the mesh size by an appropriate eddy viscosity model (see [13] for a review of such models). For an ideal LES calculation it is the combination of laminar and LES viscosity that is supposed to be the sole mechanism for the transfer of energy to the sub-grid level through the dissipation of high frequencies. Unfortunately many schemes exhibit large amounts of *numerical* diffusion at high frequencies and this can have a disastrous effect on LES since it allows energy

to be transferred independently of the LES model itself. As a result, a convective scheme that is well-suited to LES must have minimal dissipation at high frequencies. Fortunately, high-frequency dispersive errors have a much smaller effect on any larger-scale structures: these modes have very short life-spans as they are effectively dissipated by turbulent viscosity and so are convected over relatively short distances. On the other hand the large scale structures themselves must be convected with both low dispersive and dissipative errors. For practical evidence of this, see Morinishi [14], who shows that non-dissipative schemes perform better than dissipative schemes on turbulent LES channel flow calculations.

Finally, we note that our aim is to compute turbulent flows in complex geometries using an *existing* parallel solver [15], and so our approach has been reasonably pragmatic: the algorithm needed to be scalable and very easy to implement within a distributed-memory environment (requiring a compact stencil, and avoiding the use of state-of-the-art iterative solvers which would be needed to ensure scalability when inverting any complicated sparse matrix systems); it also needed to be applicable to arbitrary element types. The overall design constraint was that the cost per time-step had to be limited to two or three times that of the existing second-order cell-vertex finite-volume schemes that are described in [15].

The format of the paper is as follows. In Section 2 we describe the Taylor–Galerkin (TG) schemes of Donea, Selmin, and Quartapelle and propose a new scheme for the one-dimensional advection equation that is suitable for the type of application we have in mind. In Section 3 we generalize these TG schemes for the Euler equations in two and three dimensions. We explain how the integrals appearing in the formulation can be approximated by an original method that is cheaper than well-known quadrature approaches, while maintaining discrete conservations. In Section 4 we give numerical results for basic convection problems. Numerical estimates of the order of accuracy of these schemes are given, and we describe basic test cases relating to 3D homogeneous isotropic turbulence. As the aim of the paper is to describe the scheme in detail, we do not consider the implementation of boundary conditions or give results for more challenging test cases, although we intend to report on this in future publications.

2. TAYLOR–GALERKIN SCHEMES FOR THE ONE-DIMENSIONAL ADVECTION EQUATION

2.1. *The ETG Scheme*

The Euler–Taylor–Galerkin (ETG) scheme was the first third-order TG scheme proposed by Donea [9]. We derive it here for the 1D advection equation,

$$u_t = -cu_x, \qquad x \in \Omega, \tag{1}$$

where c is a constant, and suitable initial and boundary conditions are imposed. The method is based on a third-order Taylor expansion in time,

$$\frac{u^{n+1} - u^n}{\Delta t} = u_t^n + \frac{\Delta t}{2} u_{tt}^n + \frac{\Delta t^2}{6} u_{ttt}^n + O(\Delta t^3), \tag{2}$$

which is that used by the classical Lax–Wendroff scheme with a third derivative term added on the right-hand side. The second derivative u_{tt} is replaced by a second derivative in space using Eq. (1) twice,

$$u_{tt} = (-cu_x)_t = -c(u_t)_x = c^2 u_{xx}. \tag{3}$$

The third-order derivative is then approximated in a hybrid manner using forward Euler time-stepping,

$$u_{ttt} = c^2(u_t)_{xx} \simeq c^2\left(\frac{u^{n+1}-u^n}{\Delta t}\right)_{xx}. \tag{4}$$

After replacing all temporal derivatives by spatial derivatives, this results in the semi-discrete form,

$$\left(1-\frac{c^2\Delta t^2}{6}\partial_{xx}\right)\left(\frac{u^{n+1}-u^n}{\Delta t}\right) = -cu_x^n + \frac{c^2\Delta t}{2}u_{xx}^n. \tag{5}$$

To obtain a fully discrete approximation, the Galerkin method is applied to the above equation,

$$\left\langle\left(1-\frac{c^2\Delta t^2}{6}\partial_{xx}\right)\left(\frac{u^{n+1}-u^n}{\Delta t}\right), \phi_i\right\rangle = \left\langle -cu_x^n + \frac{c^2\Delta t}{2}u_{xx}^n, \phi_i\right\rangle, \tag{6}$$

where $\langle a, b\rangle$ denotes the L_2 inner product $\int ab\,dV$, and ϕ_i is a test function taken from a suitably chosen finite-element subspace. A P^1 finite element approximation is obtained by integrating (6) by parts and choosing piecewise linear functions satisfying

$$\phi_j(x_i) = \delta_{ij}$$
$$\sum_j \Phi_j(x) = 1, \qquad \forall\, x \in \Omega,$$

where $x_i = x_0 + i\,\Delta x$ denotes a mesh coordinate (limiting our present discussion to regular meshes). This finally gives the discrete scheme for the nodal values U_j^n,

$$\left[M - \frac{C^2}{6}\delta^2\right](U_j^{n+1} - U_j^n) = -C\Delta_0 U_j^n + \frac{1}{2}C^2\delta^2 U_j^n, \tag{7}$$

where $C = c\Delta t/\Delta x$ is the Courant number, Δ_0, δ^2 are the centred first- and second-order spatial differencing operators, and M is the mass-matrix,

$$\Delta_0 U_j = \frac{1}{2}(U_{j+1} - U_{j-1}) \tag{8}$$
$$\delta^2 U_j = U_{j+1} - 2U_j + U_{j-1} \tag{9}$$
$$MU_j = \frac{1}{6}(U_{j+1} + 4U_j + U_{j-1}). \tag{10}$$

2.2. *TTG3 and TTG4A Schemes*

In [16], Donea *et al.* carried out the 2D stability analysis of the ETG scheme for bilinear elements. They found that although the CFL condition reads $C < 1$ in 1D, it becomes $C < \frac{1}{2}$ in 2D and $C < \frac{1}{3}$ in 3D, where C is now the CFL number based on the wave speed in a given direction and the maximum distance across the cell in that direction. To overcome this,

Selmin and Quartapelle [10, 17], proposed a family of two-step Taylor–Galerkin schemes called TTG. These are derived from the two-step approximation

$$\tilde{u}^n = u^n + \frac{1}{3}\Delta t u_t^n + \alpha \Delta t^2 u_{tt}^n, \tag{11}$$

$$u^{n+1} = u^n + \Delta t u_t^n + \frac{1}{2}\Delta t^2 \tilde{u}_{tt}^n, \tag{12}$$

which also avoids the need for a modified mass matrix such as that found in the ETG scheme (7). On regular meshes, $\alpha = \frac{1}{9}$ gives a third-order scheme called TTG3 whose phase error is exactly that of the ETG scheme; the choice $\alpha = \frac{1}{12}$ gives a fourth-order scheme called TTG4A. The stability limit is $C < 0.854$ for TTG3 and $C < 1$ for TTG4A for all dimensions. Thus, the higher cost per time-step of these two-step methods may be off-set by the larger time-step that is allowed. Quartapelle and Selmin also carried out 1D and 2D test cases in [10] and showed that the TTG schemes give solutions that are very similar to those of the ETG scheme.

2.3. *TTGC Schemes*

Unfortunately, we have found that the ETG and TTG schemes are too dissipative at intermediate and high frequencies and that these schemes are therefore unsuitable for practical LES applications. As a result, a new class of two-step Taylor–Galerkin schemes has been developed that gives third-order accuracy with less overall dissipation.

We consider the six parameter family of schemes,

$$\tilde{u}^n = u^n + \alpha \Delta t u_t^n + \beta \Delta t^2 u_{tt}^n, \tag{13}$$

$$u^{n+1} = u^n + \Delta t\left(\theta_1 u_t^n + \theta_2 \tilde{u}_t^n\right) + \Delta t^2\left(\epsilon_1 u_{tt}^n + \epsilon_2 \tilde{u}_{tt}^n\right). \tag{14}$$

We note that it is possible to move the second-order derivative terms of (13) and (14) to the left-hand side and to treat these terms within a modified mass matrix, in a manner analogous to the definition of the ETG scheme or the multi-step schemes derived by Oden *et al.* [11, 12]. This approach can lead to fourth-order schemes, and even unconditionally stable schemes, although it can be much more expensive to implement and so will not be considered here.

After discretising the above equations using linear elements and the Galerkin scheme, we perform a Fourier transform which gives the amplification factor

$$\tilde{z}(p) = 1 + \frac{1}{\hat{M}}(-\alpha C \hat{\Delta}_0 + \beta C^2 \hat{\delta}^2), \tag{15}$$

$$z(p) = 1 + \frac{1}{\hat{M}}(-(\theta_1 + \theta_2 \tilde{z}) C \hat{\Delta}_0 + (\epsilon_1 + \epsilon_2 \tilde{z}) C^2 \hat{\delta}^2), \tag{16}$$

where $\hat{\Delta}_0$, $\hat{\delta}^2$, $\hat{M}$, are the Fourier transforms of Δ_0, δ^2, M given by the equations (see (8), (9), and (10))

$$\hat{\Delta}_0(p) = I \sin(p),$$

$$\hat{\delta}^2(p) = -4\left(\sin\left(\frac{p}{2}\right)\right)^2,$$

$$\hat{M}(p) = 1 - \frac{2}{3}\sin\left(\frac{p}{2}\right)^2,$$

and $p = k\Delta x$ is the non-dimensional frequency. A Taylor expansion to third order in p gives

$$z(p) = 1 - a_1 ICp - a_2 C^2 p^2 + a_3 IC^3 p^3 + o(p^3), \tag{17}$$

with

$$\begin{aligned} a_1 &= \theta_1 + \theta_2, \\ a_2 &= \epsilon_1 + \epsilon_2 + \alpha(1 - \theta_1), \\ a_3 &= \frac{1}{2}\alpha(1 - 2\epsilon_1) + (1 - \theta_1)(\beta - \alpha^2), \end{aligned}$$

and we note that a third-order accurate scheme requires the coefficients a_i to satisfy $a_i = \frac{1}{i!}$ for $i = 1, 2, 3$. Clearly, the two-step Taylor–Galerkin schemes described in Subsection 2.2 satisfy these conditions—for instance, the TTG4A scheme is defined by $\alpha = \frac{1}{3}$, $\beta = \frac{1}{12}$, $\theta_1 = 1$, $\theta_2 = 0$, $\epsilon_1 = 0$, and $\epsilon_2 = \frac{1}{2}$.

We now have three equations and six free parameters, and so additional constraints need to be imposed. The dissipative property of the scheme can be assessed by determining the dissipation of the amplification factor at the highest mesh frequency $p = \pi$. In this case, we have

$$\hat{\Delta}_0(\pi) = 0, \quad \hat{\delta}^2(\pi) = -4, \quad \hat{M}(\pi) = \frac{1}{3}$$

and $z(\pi)$ is given exactly by

$$z(\pi) = 1 - 12C^2[\epsilon_1 + \epsilon_2(1 - 12\beta C^2)].$$

It can be seen that setting $\epsilon_1 = \epsilon_2 = 0$ leads to no dissipation at all for this mode ($z(\pi) = 1$), as is the case for well-known Galerkin/Runge–Kutta schemes. Thus, at least one of these two coefficients has to be non-zero in order to keep a minimum dissipation at high frequencies.

As our aim is to derive a third-order scheme that is as cheap as possible, with less dissipation than those described in the previous section, we make the following choices:

- We demand that the second derivative term u_{tt} be calculated only once per time-step. If we wish to keep a dissipative-like term at both steps of the iteration, β cannot be zero so u_{tt} has to be calculated during the first step and ϵ_2 can be set to zero.
- We impose the condition $\theta_1 = 0$ since we also wish to avoid the additional cost of storing u_t^n from step one to step two (it may also be shown that θ_1 has little practical effect on the phase and dissipative properties of the scheme).

Setting $\gamma = \epsilon_1$, with $\theta_1 = 0$ and $\epsilon_2 = 0$, the three initial constraints now become

$$\alpha = \frac{1}{2} - \gamma, \qquad \beta = \frac{1}{6}, \tag{18}$$

and the two-step scheme reads

$$\tilde{u}^n = u^n + \alpha \Delta t u_t^n + \beta \Delta t^2 u_{tt}^n, \tag{19}$$

$$u^{n+1} = u^n + \Delta t \tilde{u}_t^n + \gamma \Delta t^2 u_{tt}^n. \tag{20}$$

Equations (19) and (20) define a family of schemes that depend on a single parameter γ, which may be interpreted as a measure of the dissipation at high frequencies, as shown by

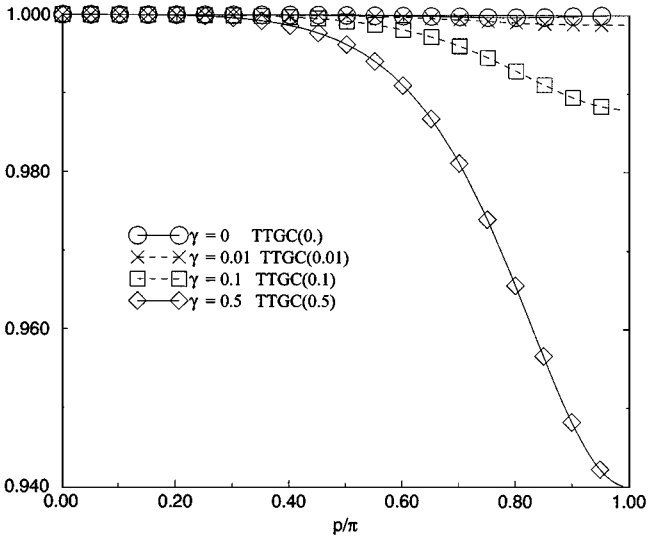

FIG. 1. Dissipation error of different TTGC schemes at CFL = 0.1.

the amplification factor at the maximal frequency $p = \pi$,

$$z(\pi) = 1 - 12\gamma C^2.$$

As γ tends to zero, the dissipation of high frequency modes also tends to zero, as shown graphically in Fig. 1. If $\gamma = 0$, the second step of the scheme is formally identical to a step of a multi-step Galerkin scheme, leading to the node-to-node oscillations discussed in the Introduction. Figure 2 shows that the dispersion error is nearly independent of γ, at least at low CFL numbers. Figure 3 shows the maximum CFL condition in 1D for $\gamma \in [0, 1]$. It can be seen that in practice only small values of γ $(0 < \gamma \leq 0.2)$ lead to acceptable CFL limits. Negative values of γ lead to an instable scheme.

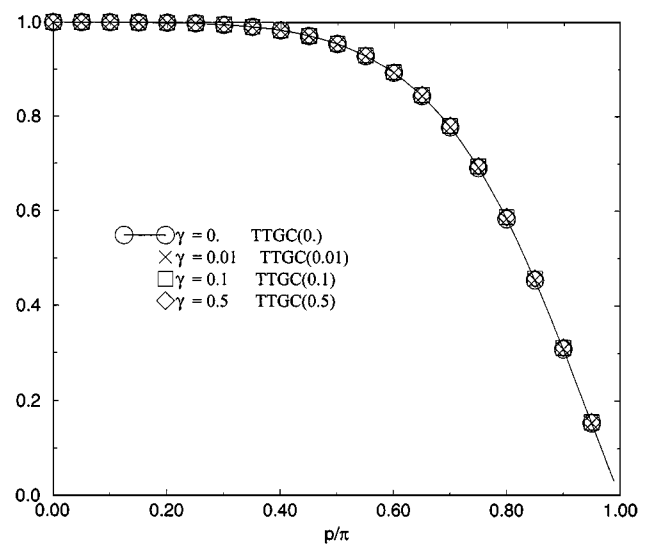

FIG. 2. Dispersion error of different TTGC schemes at CFL = 0.1.

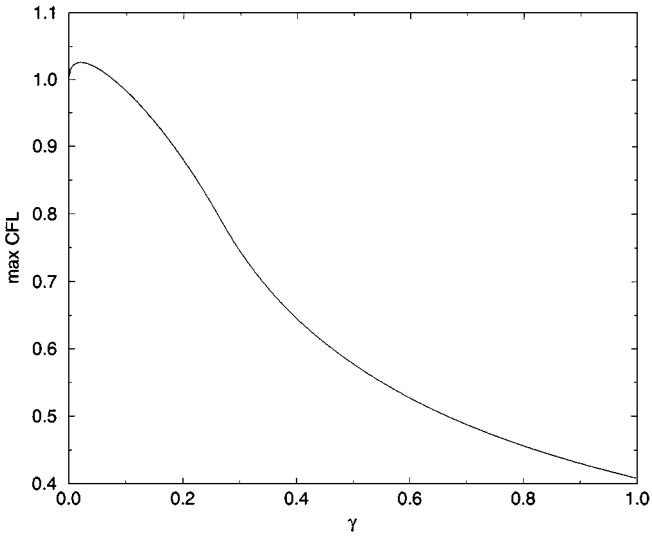

FIG. 3. TTGC(γ) stability domain for the 1D advection equation with $\gamma \in [0, 1]$.

Finding a single *optimal* value for γ across all CFL numbers has not been addressed in the present work because it is somewhat difficult to define precisely what is meant by this in the context of LES calculations (where dissipation is needed for non-linear stability but an excess of dissipation strongly degrades the turbulence characteristics).

Numerically, we have found that $0 < \gamma \leq 0.05$ gives a much less dissipative scheme than FV/LW, ETG, or TTG4A over the whole frequency spectrum for small CFL numbers (as can be seen in Fig. 4) whereas it is comparable to other third-order TG schemes for high CFL numbers and long to intermediate wavelengths (see Fig. 5). Nonetheless, for $\gamma > 0$ the scheme remains more dissipative at high frequencies than the three-step Galerkin scheme, as shown by the numerical tests of Section 4. The dispersion error is very similar to that of other TG schemes, especially at low CFL numbers (see Figs. 6 and 7) and brings a

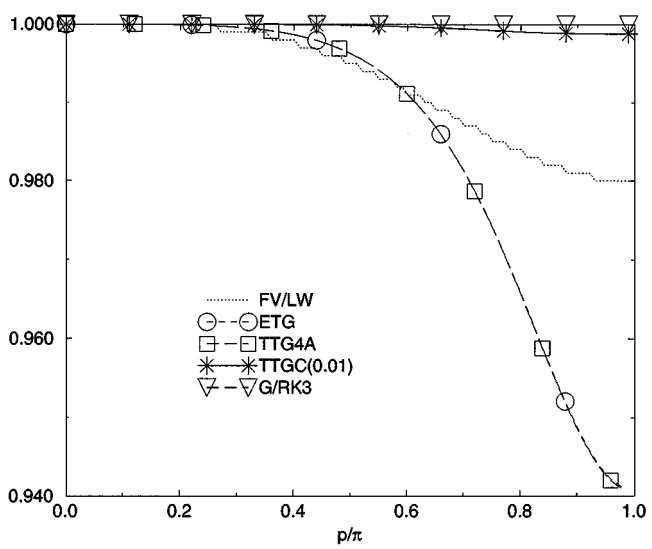

FIG. 4. Dissipation error of LW and TG schemes at CFL = 0.1.

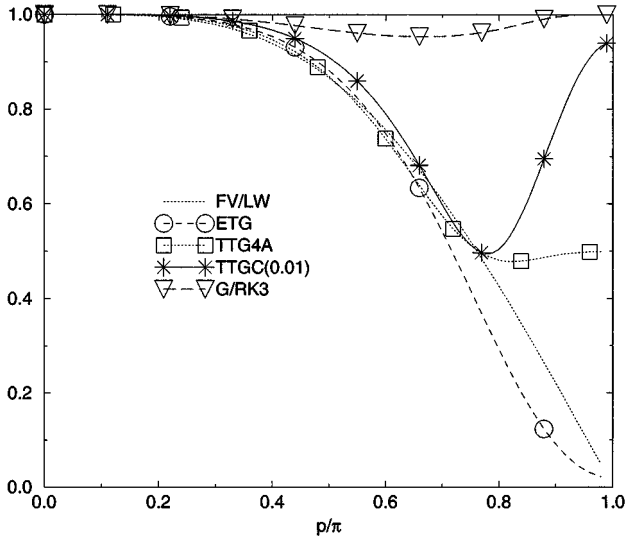

FIG. 5. Dissipation error of LW and TG schemes at CFL = 0.7.

clear improvement over FV/LW or FV/RK3 schemes. In the following we will denote the generic formulation as TTGC (following the naming convention adopted for the TTG4A and TTG4B schemes of Quartapelle *et al.*); TTGC(γ') will refer to the particular case $\gamma = \gamma'$.

3. MULTI-DIMENSIONAL TTG SCHEMES FOR THE EULER EQUATIONS

3.1. *General Formulation*

We now consider the three-dimensional Euler equations written in conservative form,

$$u_t + \nabla \cdot F = 0 \tag{21}$$

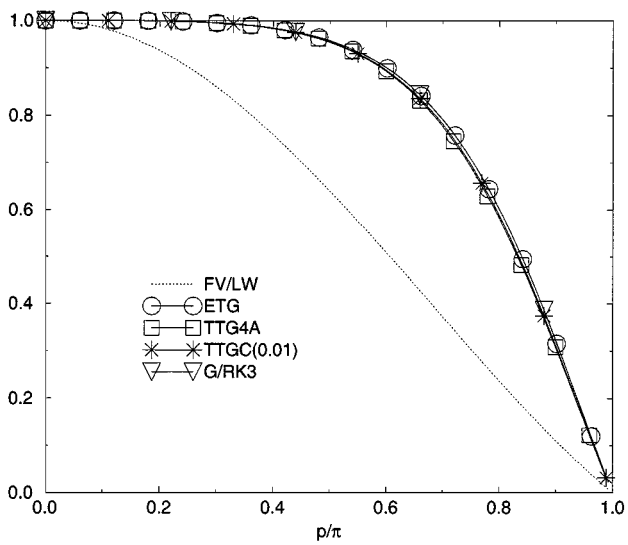

FIG. 6. Dispersion error of LW and TG schemes at CFL = 0.1.

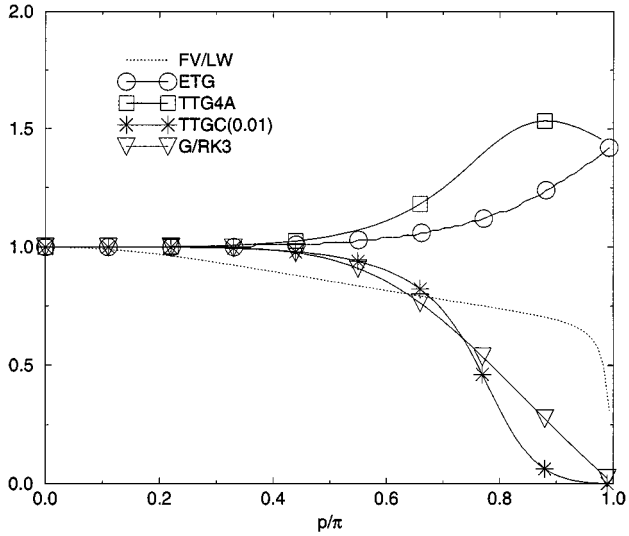

FIG. 7. Dispersion error of LW and TG schemes at CFL = 0.7.

with $u^T = (\rho, \rho u_1, \rho u_2, \rho u_3, \rho E)$, where ρ is the density, $q^T = (u_1, u_2, u_3)$ denotes the velocity field, E is the total energy per unit mass, and $F = (\mathrm{f}, \mathrm{g}, \mathrm{h})$ is the 5×3 matrix of inviscid fluxes. Replacing the temporal derivatives of Eqs. (19) and (20) using (21) and

$$u_{tt} = -(\nabla \cdot F)_t = -\nabla \cdot F_t = \nabla \cdot ((A, B, C)u_t), \tag{22}$$

where A, B, C are the 5×5 flux Jacobians,

$$A(u) = \frac{\partial f}{\partial u}, \qquad B(u) = \frac{\partial g}{\partial u}, \qquad C(u) = \frac{\partial h}{\partial u}, \tag{23}$$

we finally obtain

$$\tilde{u}^n = u^n - \alpha \Delta t \nabla \cdot F^n + \beta \Delta t^2 \nabla \cdot [(A, B, C)(\nabla \cdot F^n)], \tag{24}$$

$$u^{n+1} = u^n - \Delta t \nabla \cdot \tilde{F}^n + \gamma \Delta t^2 \nabla \cdot [(A, B, C)(\nabla \cdot F^n)], \tag{25}$$

where the divergence $\nabla \cdot F = f_x + g_y + h_z$ is a 5×1 matrix and $(A, B, C)(\nabla \cdot F) = (A\nabla \cdot F, B\nabla \cdot F, C\nabla \cdot F)$ is a 5×3 matrix.

After applying the Galerkin method to Eqs. (24) and (25) and integrating the second-order operator by parts, the scheme becomes

$$\int_\Omega \tilde{R}^n \Phi_i \, dV = -\alpha L_i(U^n) - \beta \Delta t L L_i(U^n), \tag{26}$$

$$\int_\Omega R^{n+1} \Phi_i \, dV = -L_i(\tilde{U}^n) - \gamma \Delta t L L_i(U^n), \tag{27}$$

with

$$\tilde{R}^n = \frac{\tilde{U}^n - U^n}{\Delta t},$$

$$R^{n+1} = \frac{U^{n+1} - U^n}{\Delta t},$$

$$L_i(U^n) = \int_\Omega \nabla \cdot F(U^n) \Phi_i \, dV, \tag{28}$$

$$LL_i(U^n) = \int_\Omega (A, B, C)\nabla \cdot F(U^n)\nabla\Phi_i \, dV - \int_{\partial\Omega} \Phi_i(A, B, C)\nabla \cdot F(U^n) \, dS, \quad (29)$$

where the surface vector dS is 3×1 matrix and we have chosen suitable scalar test functions Φ_i. $U, \tilde{U}$ are expressed as a sum of these test-functions, e.g.,

$$\begin{aligned} U^n(x) &= \sum_j \Phi_j(x) U_j^n, \\ R^n(x) &= \sum_j \Phi_j(x) R_j^n, \end{aligned} \quad (30)$$

and the left-hand side of (26) then becomes

$$\begin{aligned} \int_\Omega \tilde{R}^n \Phi_i \, dV &= \sum_j \left(\int_\Omega \Phi_i \Phi_j \, dV \right) \tilde{R}_j^n \\ &= \sum_j M_{ij} \tilde{R}_j^n. \end{aligned}$$

The TTG scheme may be rewritten in matrix form, with U^n, $\tilde{U}^n$, $\tilde{R}^n$, R^{n+1} now designating the vectors of nodal values, and M the mass-matrix,

$$M\tilde{R}^n = \tilde{H}(U^n), \quad (31)$$

$$MR^{n+1} = H(U^n, \tilde{U}^n), \quad (32)$$

with H and $\tilde{H}$ defined as

$$\begin{aligned} \tilde{H}(U^n) &= -\alpha L(U^n) - \beta \Delta t L L(U^n), \\ H(U^n, \tilde{U}^n) &= -L(\tilde{U}^n) - \gamma \Delta t L L(U^n). \end{aligned}$$

As the CFL condition for TTGC is less than one, the number of time-steps required by a typical LES will be very large. This makes the CPU cost per iteration a crucial factor for this scheme, as for all explicit time-stepping schemes. The exact inversion of the (positive-definite) mass-matrix M would involve storing a large full matrix and is therefore not of practical interest, especially for unstructured meshes; instead we report to approximate inversion techniques using a very simple iterative method. In [9], Donea proposed a two-step explicit version which remains third-order and nearly preserves the phase accuracy of the original one-step implicit version. This involves approximating the matrix inversion by the well-known Jacobi method. Similarly, the p-step explicit version of the TTGC scheme becomes

$$\begin{aligned} (\tilde{R}^n)^{(0)} &= D^{-1}\tilde{H}(U^n), \\ (\tilde{R}^n)^{(k)} &= (\tilde{R}^n)^{(0)} - D^{-1}(M - D)(\tilde{R}^n)^{(k-1)}, \qquad k = 1, p, \\ (R^{n+1})^{(0)} &= D^{-1}H\big(U^n, (\tilde{U}^n)^{(p)}\big), \\ (R^{n+1})^{(k)} &= (R^{n+1})^{(0)} - D^{-1}(M - D)(R^{n+1})^{(k-1)}, \qquad k = 1, p, \end{aligned} \quad (33)$$

where D is the diagonally lumped mass matrix,

$$\begin{aligned} D_{ii} &= \sum_j M_{ij}, \\ D_{ij} &= 0 \qquad \text{for } i \neq j. \end{aligned}$$

Note that we have chosen to use the mass-lumped matrix and not the diagonal of M because it may be shown that convergence is assured on arbitrary (tetrahedral) meshes when the mass-lumped matrix is used [18]. An alternative to this approach would be to use a diagonally preconditioned conjugate-gradient technique [19], which also has favourable convergence properties for this problem and avoids the need to store a pre-conditioning matrix, although it is slightly more costly to implement due to the additional vector–vector products that are required.

Since the other TG schemes, as well as the G/RK3 scheme, may also be expressed as linear combinations of the operators L and LL, the implementation of this family of schemes is straightforward and similar techniques may be used in all cases. By performing a Fourier analysis following [9], we may show analytically that all of the schemes remain third-order accurate when the mass-matrix is inverted approximately using one or more steps of Jacobi, at least for regular infinite meshes. For the multi-dimensional Euler equations, no analytical proof of the order is given here, although the numerical estimate of the order presented in Subsection 4.1 shows that third order is still attained on regular meshes. Indeed, we shall demonstrate that only two iterations ($p = 2$) are required to obtain solutions that are very close to those given by exact matrix inversion. Figures 8 and 9 illustrate this by comparing dispersion and dissipation errors for the one-dimensional problem (the reader should note the vertical scale of Fig. 9).

3.2. *Application to Linear and Bilinear Elements*

The practical computation of the operators L and LL can be done element by element,

$$L_i(U^n) = \sum_{c, i \in \Omega_c} L_i(U^n)|_c,$$

$$LL_i(U^n) = \sum_{c, i \in \Omega_c} LL_i(U^n)|_c,$$

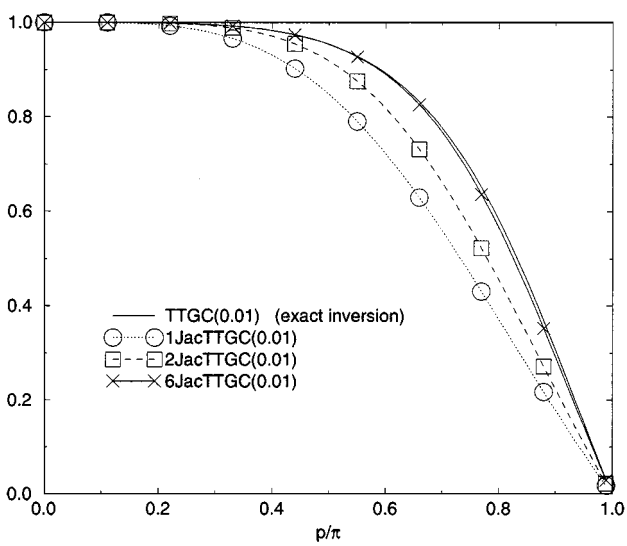

FIG. 8. Dispersion error for nJacTTGC(0.01) scheme at CFL = 0.1.

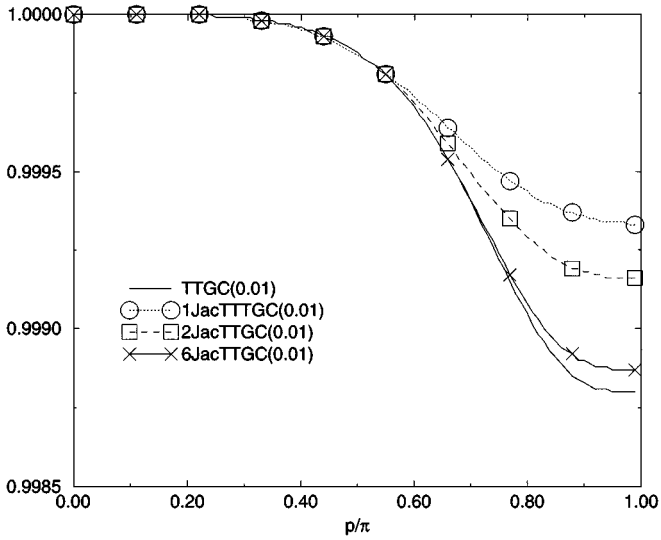

FIG. 9. Dissipation error for nJacTTGC(0.01) scheme at CFL = 0.1.

where

$$L_i(U^n)|_c = \int_{\Omega_c} \Phi_i \nabla \cdot F \, dV,$$

$$LL_i(U^n)|_c = \int_{\Omega_c} \Phi_{ix} A \nabla \cdot F \, dV + \int_{\Omega_c} \Phi_{iy} B \nabla \cdot F \, dV + \int_{\Omega_c} \Phi_{iz} C \nabla \cdot F \, dV.$$

However, their exact evaluation involves the continuous functions $F(U^n)$, $A(U^n)$, $B(U^n)$, and $C(U^n)$ defined over each element Ω_c, recalling that U^n itself is a linear combination of the test-functions (see Eq. (30)). For the Euler equations, the Jacobians and the flux are complicated nonlinear functions of U and so it is convenient to make the following approximations:

- We use a product approximation to express the flux F as a sum of test-functions,

$$F^n(x) = \sum_j \Phi_j(x) F_j^n, \tag{34}$$

which gives

$$\nabla \cdot F^n(x) = \sum_j F_j^n \nabla \Phi_j(x).$$

- The Jacobians are taken to be constant over each element and are approximated using the average value of the vertex values U_j^n, $j \in \Omega_c$. Note that this approximation only appears in the LL term.

The expressions for L and LL can then be simplified,

$$L_i(U^n)|_c = \sum_{j \in \Omega_c} F_j \Theta_{ij}|_c, \tag{35}$$

$$LL_i(U^n)|_c = \sum_{j\in\Omega_c}\left(AF_j\int_{\Omega_c}\Phi_{ix}\nabla\Phi_j\,dV + BF_j\int_{\Omega_c}\Phi_{iy}\nabla\Phi_j\,dV + CF_j\int_{\Omega_c}\Phi_{iz}\nabla\Phi_j\,dV\right)$$

$$= (A, B, C)\left(\sum_{j\in\Omega_c}F_j\Psi_{ij}|_c\right), \tag{36}$$

where Θ and Ψ are defined over each element as

$$\Theta_{ij}|_c = \int_{\Omega_c}\Phi_i\nabla\Phi_j\,dV, \tag{37}$$

$$\Psi_{ij}|_c = \int_{\Omega_c}\nabla\Phi_j(\nabla\Phi_i)^T\,dV. \tag{38}$$

For quadrilaterals in 2D, or prisms, pyramids or hexahedra in 3D, the test-functions appearing in the above integrals may be expressed as bilinear or trilinear polynomials of the canonical coordinates $\tilde{x}$ of some reference element in computational space, whereas they can be fractional polynomials of the original coordinates x. They are therefore calculated over the reference element $\tilde{\Omega}_c$ by using the transformation

$$R : \tilde{\Omega}_c \to \Omega_c,$$
$$\tilde{x} \to x = \sum_i x_i\Phi_i(\tilde{x}),$$

and (37) and (38) then become

$$\Theta_{ij}|_c = \int_{\tilde{\Omega}_c}\Phi_i T\nabla\Phi_j\,dV, \tag{39}$$

$$\Psi_{ij}|_c = \int_{\tilde{\Omega}_c}|P|^{-1}T\nabla\Phi_j\nabla\Phi_i^T T^T\,dV, \tag{40}$$

where $P = \frac{\partial x}{\partial\tilde{x}}$ is the Jacobian of the transformation R, and $T = |P|(P^T)^{-1}$.

3.2.1. Linear formulation. In the case of triangular or tetrahedral elements, the test-functions are linear functions of the coordinates and the transformation R is itself linear (i.e., P is constant). Consequently, T and $\nabla\Phi_i$ are constant over each element and can be taken out of the integrals (39) and (40). Then we have

$$\nabla\Phi_j = -\frac{N_j}{DV_c}, \tag{41}$$

where the 3×1 matrix N_j is the outward normal to the face opposite to node j, scaled by the surface area of the face; D is the space dimension and V_c is the volume of the element. The integral of the test function itself reduces to

$$\int_{\Omega_c}\Phi_j\,dV = \frac{V_c}{I_c}, \qquad \forall j\in\Omega_c \tag{42}$$

where I_c is the number of vertices in the element Ω_c: 3 for triangles, 4 for tetrahedra. Finally, L_i^c and LL_i^c take the simple forms

$$L_i(U^n)|_c = \frac{V_c}{I_c}(\nabla\cdot F)_c, \tag{43}$$

$$LL_i(U^n)|_c = -\frac{1}{D}(A, B, C)(\nabla\cdot F)_c N_i, \tag{44}$$

where

$$(\nabla \cdot F)_c = -\frac{1}{DV_c}\left(\sum_{j\epsilon\Omega_c} F_j N_j\right). \tag{45}$$

Although the expressions (43) and (44) correspond to the exact integration of (39) and (40), we note that these expressions are exactly those used in our basic finite-volume solver [20].

3.2.2. Bi/tri-linear formulation. In the case of bi/tri-linear elements such as quadrilaterals, prisms, pyramids, and hexahedra, T and $\nabla\Phi_i$ are no longer constant within each cell, and so these cannot be taken out of the integrals (39) and (40). Their approximate integration is commonly performed using quadrature, although this can be expensive (simple one-point quadrature is not considered as this leads to spurious solution modes, whereas a full $2 \times 2 \times 2$ quadrature would require nearly eight times as much work as the former); care must also be taken in order to maintain the essential property of discrete flux conservation. The solution adopted here is to consider both T and $|P|$ to be constant over each element, as in the linear case. The approximation is based on the fact that T and $|P|$ are indeed constant when the element is regular, that is, for parallelograms in 2D or parallelepipeds in 3D. For irregular elements, we need to define some average of T and $|P|$, denoted $\bar{T}$ and $|\bar{P}|$. In the present work, we have chosen $\bar{T} = T(x_G)$ where x_G is the barycentre of the element. Similarly, $|\bar{P}|$ is defined

$$\int_{\Omega_c} 1\, dV = \int_{\tilde{\Omega}_c} |P|\, d\tilde{V} \simeq |\bar{P}| \int_{\tilde{\Omega}_c} d\tilde{V}.$$

As we have arbitrarily chosen $\int_{\tilde{\Omega}_c} d\tilde{V} = I_c$, we find

$$|\bar{P}| = V_c/I_c.$$

In order to guarantee the conservation property (see the Appendix for the proof) we split Θ_{ij} into two terms,

$$\Theta_{ij}|_c = \Theta_{ij}^{(0)}\big|_c + \Theta_{ij}^{(1)}\big|_c,$$

where

$$\Theta_{ij}^{(0)}\big|_c = \int_{\Omega_c} \Phi_i \overline{\nabla\Phi}_j\, dV, \tag{46}$$

$$\Theta_{ij}^{(1)}\big|_c = \int_{\Omega_c} \Phi_i (\nabla\Phi_j - \overline{\nabla\Phi}_j)\, dV, \tag{47}$$

and

$$\overline{\nabla\Phi}_j = \frac{1}{V_c}\int_{\Omega_c} \nabla\Phi_j\, dV = \frac{1}{V_c}\int_{\tilde{\Omega}_c} T\nabla\Phi_j\, d\tilde{V}.$$

We now define

$$\overline{\overline{\nabla\Phi}}_j = \frac{1}{V_c}\bar{T}\int_{\tilde{\Omega}_c} \nabla\Phi_j\, d\tilde{V} \tag{48}$$

and note that for regular elements

$$\overline{\nabla\Phi}_j = \overline{\overline{\nabla\Phi}}_j = (\nabla\Phi_j)_{FV},$$

with

$$(\nabla \Phi_j)_{FV} = \frac{1}{V_c} \int_{\partial \Omega_c} \Phi_j \, dS. \tag{49}$$

For irregular elements with non-coplanar quadrilateral faces, we define $(\nabla \Phi_j)_{FV}$ to be an approximation of the surface integral of (49). This involves triangulating the face, assuming linear variation of Φ over the triangle, and then taking the mean of the two possible triangulations [20]. We then approximate $\overline{\nabla \Phi}_j$ by $(\nabla \Phi_j)_{FV}$ in Eq. (46), and by $\overline{\overline{\nabla \Phi}}_j$ in Eq. (47),

$$\Theta_{ij}^{(0)}\big|_c \simeq \left(\int_{\Omega_c} \Phi_i \, dV \right) (\nabla \Phi_j)_{FV},$$
$$\Theta_{ij}^{(1)}\big|_c \simeq \bar{T} \tilde{\Theta}_{ij}^{(1)},$$

where $\tilde{\Theta}_{ij}^{(1)}$ is defined over the reference element,

$$\tilde{\Theta}_{ij}^{(1)} = \int_{\tilde{\Omega}_c} \Phi_i (\nabla \Phi_j - |\bar{P}| \bar{T}^{-1} \overline{\overline{\nabla \Phi}}_j) \, d\tilde{V} \tag{50}$$
$$= \int_{\tilde{\Omega}_c} \Phi_i \left(\nabla \Phi_j - \frac{1}{I_c} \int_{\tilde{\Omega}_c} \nabla \Phi_j \, d\tilde{V} \right) d\tilde{V}. \tag{51}$$

In the same manner Ψ_{ij} is approximated using $\bar{T}$ and $|\bar{P}|$,

$$\Psi_{ij}|_c \simeq |\bar{P}|^{-1} \bar{T} \tilde{\Psi}_{ij} \bar{T}^T,$$
$$\tilde{\Psi}_{ij} = \int_{\tilde{\Omega}_c} \nabla \Phi_j \nabla \Phi_i^T \, d\tilde{V}.$$

$\tilde{\Psi}_{ij}$, like $\tilde{\Theta}_{ij}^{(1)}$, can be calculated once and for all for each element type, since it does not depend on the mesh coordinates. $\bar{T}$, however, must be calculated for each element. When replacing $\Theta_{ij}|_c$ and $\Psi_{ij}|_c$ by their approximate expressions in Eqs. (35) and (36), L_i and LL_i become

$$L_i(U^n)|_c = \frac{V_c}{I_c} \left(\int_{\tilde{\Omega}_c} \Phi_i \, d\tilde{V} \right) (\nabla \cdot F)_{FV} + \sum_j F_j \bar{T} \tilde{\Theta}_{ij}, \tag{52}$$

$$LL_i(U^n)|_c = \frac{I_c}{V_c} (A, B, C) \left(\sum_j F_j \bar{T} \tilde{\Psi}_{ij} \bar{T}^T \right), \tag{53}$$

where

$$(\nabla \cdot F)_{FV} \approx \frac{1}{V_c} \int_{\partial \Omega_c} F \, dS,$$

the latter being evaluated using an approach similar to that defined for (49) above.

In the case of regular elements such as parallelopipeds, expressions (52) and (53) are the exact finite-element integrals appearing in Eqs. (28) and (29). On irregular elements, these expressions are only approximations of the exact finite-element formulation, but the numerical tests of the next section show that they do not appear to affect the quality of the

solutions in a significant manner, at least for practical mesh resolutions. Following similar arguments, we have approximated the mass-matrix ($\int_{\Omega_c} \Phi_i \Phi_j \, dV$) by ($V_c/I_c$)($\int_{\tilde{\Omega}_c} \Phi_i \Phi_j \, d\tilde{V}$), the expressions being identical for linear or regular, bilinear elements.

4. NUMERICAL RESULTS

4.1. *Linear Test-Case*

As a first test-case for the numerical evaluation of our scheme, a Gaussian pulse of density is convected in a uniform velocity field in two or three dimensions. Note that this test is strictly equivalent to the three-dimensional version of the convection equation (1), since the Jacobian matrices are constant and the vector equations degenerate to a single scalar equation. In 3D, the initial solution reads

$$\begin{aligned} \rho &= 1 + \exp(-100|\mathbf{r}|^2), \\ u_1 &= u_2 = u_3 = 1, \\ E &= \frac{p}{\rho(\gamma - 1)} + \frac{1}{2}|q|^2, \end{aligned}$$

where the pressure p is uniform over the whole domain, $\gamma = 1.4$, and $\mathbf{r}$ denotes the radius from the centre of the domain.

This pulse of density is initialized at time $t = 0$ in the centre of the unit periodic box ($\mathbf{x} \in [\mathbf{0}, \mathbf{1}]^{\mathbf{D}}$) discretised by N^D mesh points ($D = 2$ or 3), and thus recovers its initial position at time n, n an integer.

We present in Fig. 10 the density profile at time 1 on a hexahedral mesh of size 21^3 calculated with TTGC(0.01). This figure shows the solution on a 1D cut in the direction of propagation, i.e., between points (0, 0, 0) and (1, 1, 1) of the unit cube. All calculations with finite-element schemes are performed with the approximate inversion of the mass-matrix as described above. The TTGC scheme is therefore denoted as 2JacTTGC when 2 Jacobi iterations are performed, and similarly for the other schemes. The improvement obtained by performing two iterations of the Jacobi method instead of one is obvious in this figure; six iterations offer an even better solution but at a much higher cost. For all the following results we have therefore used two Jacobi iterations as a compromise between cost and accuracy.

Figure 11 compares the different schemes on the same mesh. We note that the dissipation and dispersion errors for third-order finite-element schemes are much smaller than those of the second-order Lax–Wendroff finite-volume scheme (FV/LW) [20] and the three-step Runge–Kutta finite-volume scheme (FV/RK3). Clearly, the particularly poor results obtained with the latter schemes are due to the relatively coarse mesh resolution of the pulse. TTG4A is the most dissipative FE scheme followed by TTGC(0.01) and G/RK3, as expected from Fig. 4. The phase accuracy on the other hand is quite similar for all FE schemes, as can be seen from Fig. 6. This calculation has also been carried out with different connectivities on a perturbed mesh (tetrahedra, pyramids, and prisms) without any significant change in the quality of the solution, as can be seen in Fig. 12. This perturbed mesh was generated by randomly moving the mesh points of the regular grid within circles of maximal radius $0.225\Delta x$. A 51^2 quad mesh is shown in Fig. 15 with the same level of perturbation and the solution obtained with this mesh is shown in Figs. 14 and 16. This calculation shows that the approximations used for bi/tri-linear elements do not negatively influence the solution in a

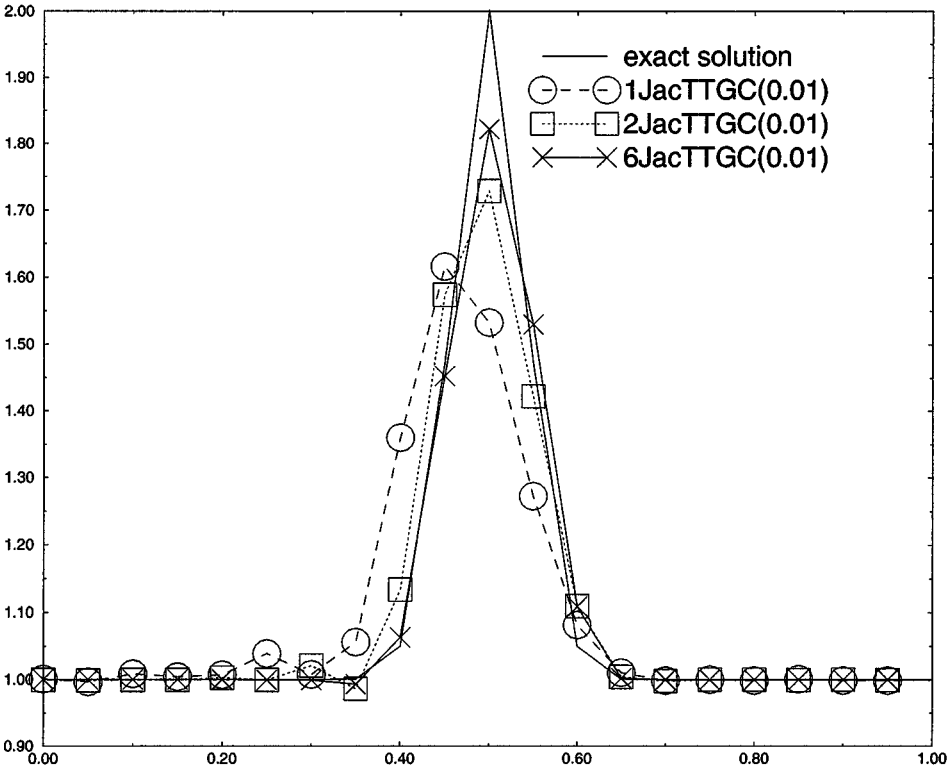

FIG. 10. Convection of a Gaussian pulse of density on a 21^3 hexahedral mesh.

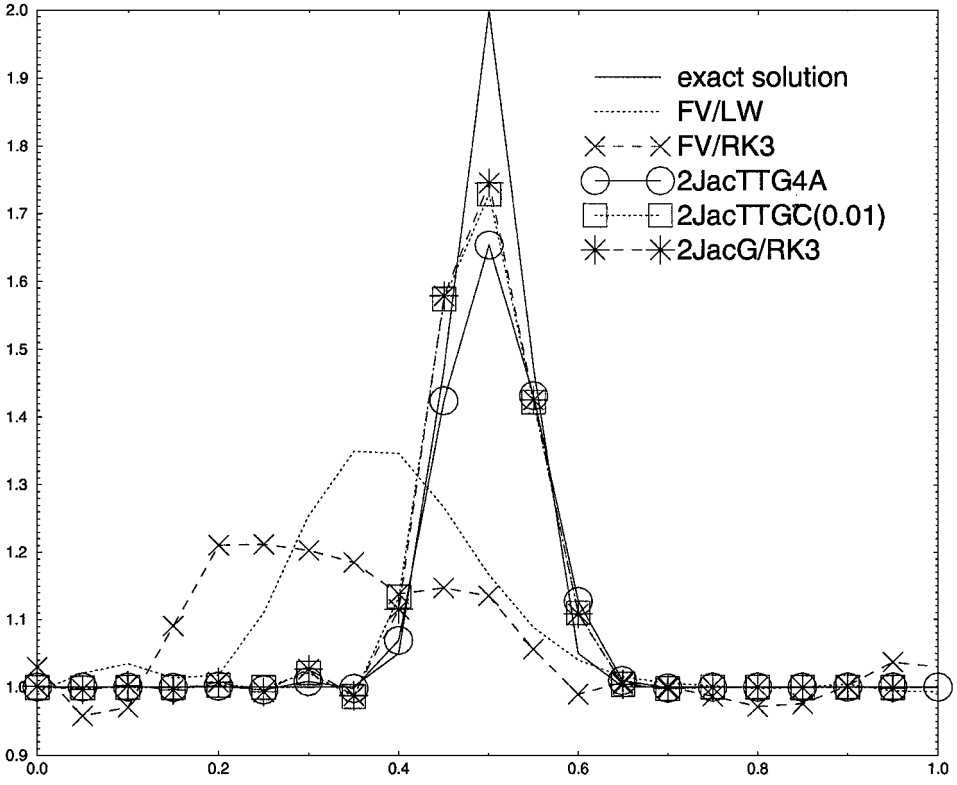

FIG. 11. Convection of a Gaussian pulse of density on a 21^3 hexahedral mesh.

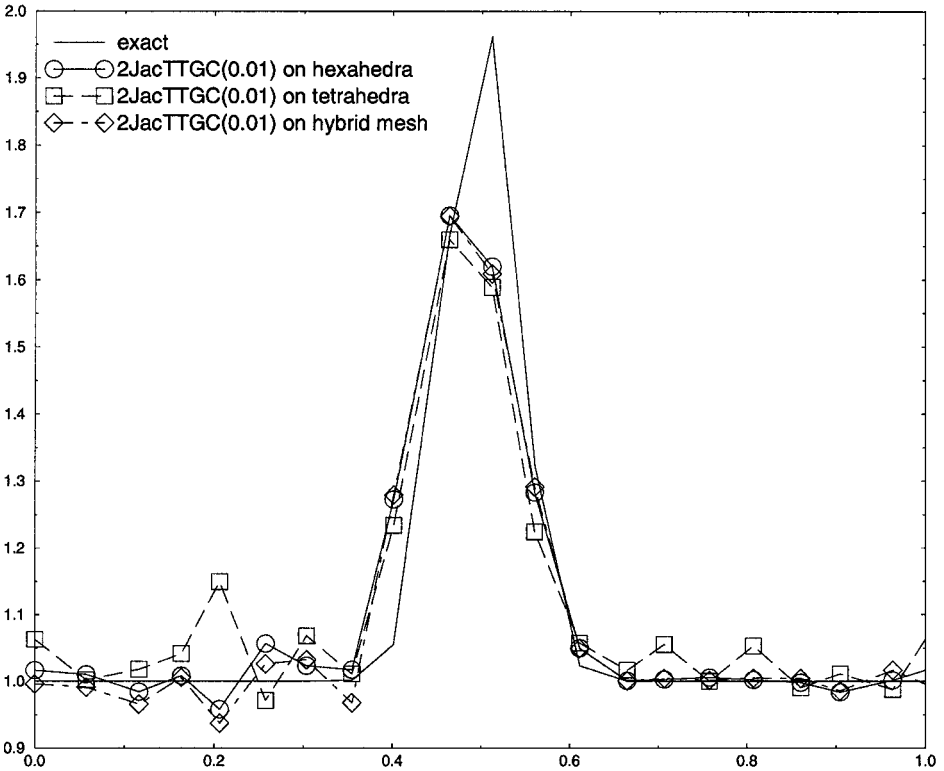

FIG. 12. Convection of a Gaussian pulse of density on a perturbed 21^3 mesh with different connectivities.

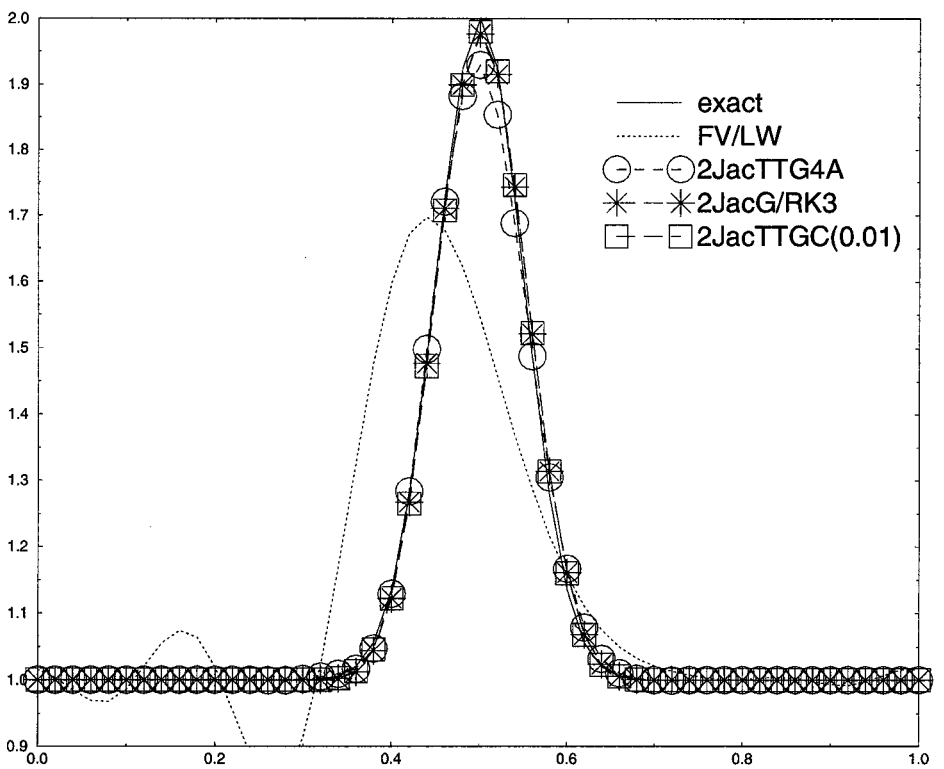

FIG. 13. Convection of a Gaussian pulse of density on a regular 51×51 quadrilateral mesh.

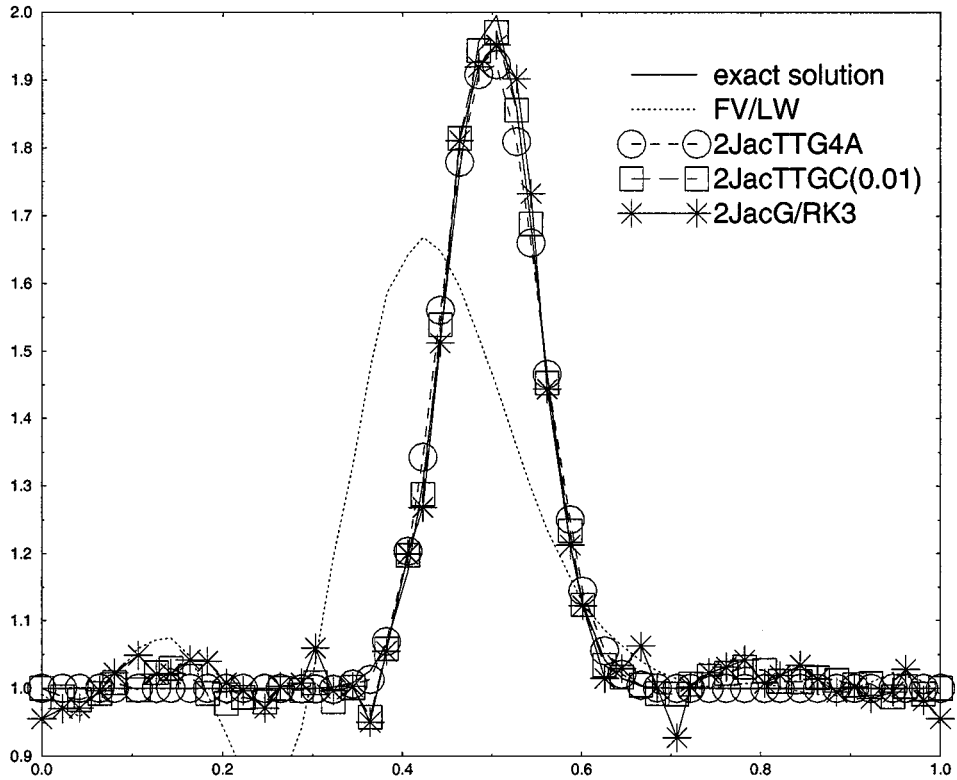

FIG. 14. Convection of a Gaussian pulse of density on a perturbed 51×51 quadrilateral mesh.

significant manner when irregular elements are used, at least for realistic mesh resolutions. The result obtained with a hybrid mesh composed of hexahedra and prisms is qualitatively similar to that obtained on a non-hybrid mesh, indicating that the use of hybrid elements does not necessarily degrade the solution accuracy for unsteady calculations.

In order to obtain a more quantitative comparison of the different schemes, we have also undertaken tests to compute their approximate orders of accuracy. The L_2 norm of the error versus the mesh spacing Δx is shown in Figs. 17 and 18, for both perturbed and regular quadrilateral meshes of sizes 15^2, 31^2, 51^2, 101^2, and 151^2. Similar tests were undertaken for triangles, using the same node distribution, as shown in Figs. 19 and 20. Table I gives the slope of the regression line which best fits the error for all of the mesh sizes considered.

TABLE I
Order Measurement for the Convection of a Gaussian Pulse of Density in Two Dimensions

Scheme	LW	2JacTTG4A	2JacTTGC (0.01)	2JacTTGC (0.05)	2JacG/RK3
Regular quad	0.8	2.7	3.5	3.7	3.6
Perturbed quad	0.74	2.1	1.3	1.7	0.87
Regular triangles	0.8	2.7	3.1	3.0	3.0
Perturbed triangles	0.8	2.4	1.8	2.1	1.4

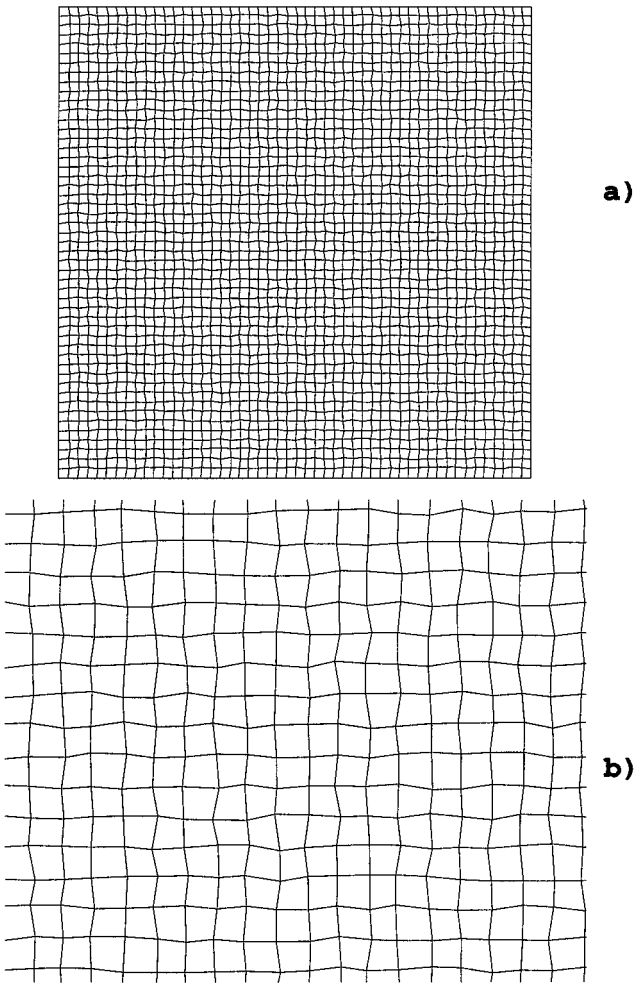

FIG. 15. A 51^2 perturbed quad mesh: (a) whole mesh, (b) detail.

Since we consider relatively coarse meshes as well much finer meshes, the slope may be interpreted as an average rate of convergence over a realistic range of mesh resolutions rather than an estimate of the order as $\Delta x \to 0$. However, in some cases (notably the regular mesh computations) the results indicate that the former is a good indication of the latter.

On regular meshes, TTGC schemes for $\gamma = 0.01$ and $\gamma = 0.05$ and G/RK3 retain third-order on triangles and even higher on quadrilaterals. The TTG4A scheme performs slightly worse (with a computed order of 2.7) and the LW scheme gives a surprisingly low order of 0.8. Note, however, that a regression fitting using the three finest meshes yields a value of 1.3 for LW and 3.9 for TTG4A on quadrilaterals, indicating that the coarser meshes do not give a good indication of the error convergence for the rapidly varying initial conditions that were used in this test.

On perturbed meshes we find that while the LW scheme retains its order, the FE schemes give reduced convergence rates. The loss in order is smaller for TTG4A and more pronounced for the other FE schemes, especially for G/RK3 on quadrilaterals, where the convergence curve flattens on the two finest meshes. We believe that this loss of accuracy is due to the creation of high-frequency oscillations on perturbed meshes which are damped by

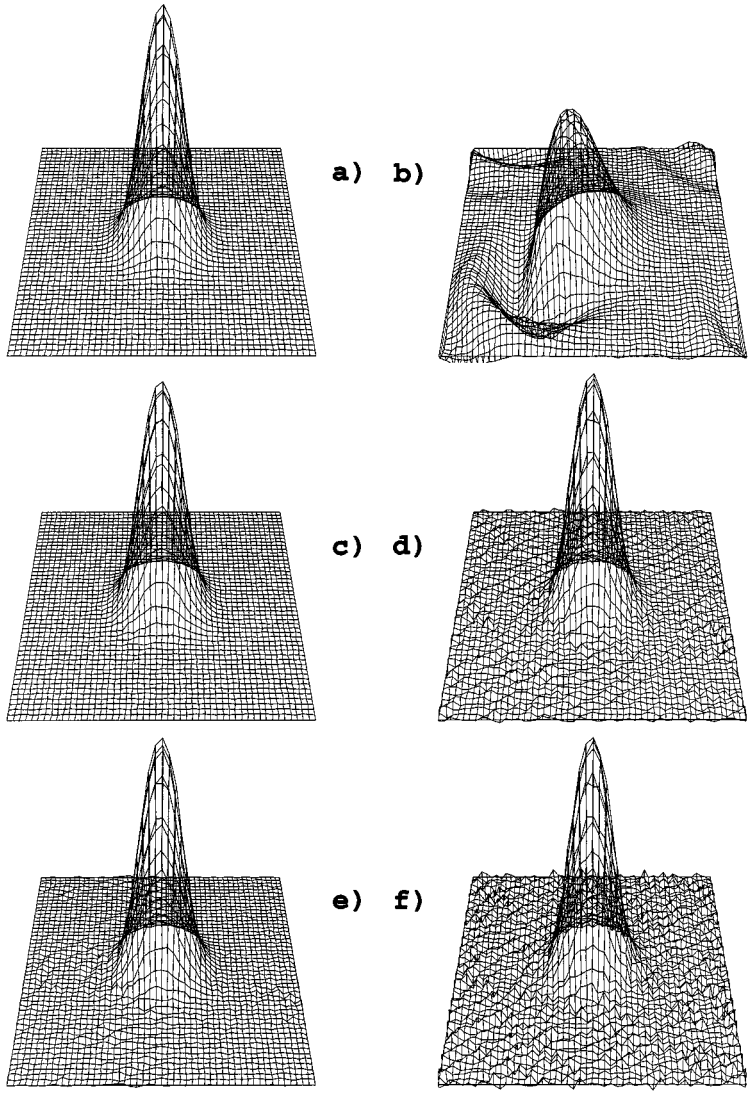

FIG. 16. Convection of a Gaussian pulse on a perturbed 51^2 quad mesh: (a) exact solution, (b) LW, (c) TTG4A, (d) TTGC(0.01), (e) TTGC(0.05), (f) G/RK3.

dissipative schemes like LW or TTG4A, but less so by TTGC or G/RK3. This is illustrated in Figs. 13 and 14 on a regular and perturbed 51^2 mesh: although solutions on the perturbed mesh show high frequency oscillations, the pulse is still accurately described. This is also illustrated in the 3D view (Fig. 16) of the same 51^2 perturbed mesh: the LW, TTG4A, and TTGC(0.05) are nearly free of these high-frequency oscillations, while TTGC(0.01) and G/RK3 show a nearly unifrom high-frequency perturbation. It can also be seen that despite the relatively good mesh resolution, the LW scheme displays a low frequency phase error (illustrated by the large undershoot behind the pulse). The results for the two TTGC schemes also illustrate how the coefficient γ directly measures the dissipation of the scheme: results on perturbed meshes are better with TTGC(0.05) than with TTGC(0.01) simply because the former damps the high frequency perturbations more effectively, while the low frequency resolution remains similar. For LES, we shall see that there is a fine balance between the

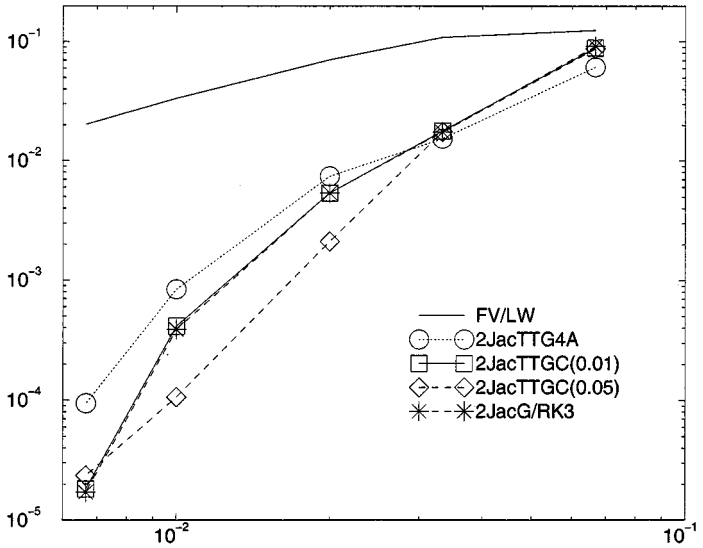

FIG. 17. L2 error versus mesh spacing on regular quadrilateral meshes for convection of a Gaussian pulse.

need to have some dissipation at high frequencies but not to overly dissipate these modes. Indeed, practical computations indicate that it is wise to have some dissipation in order to avoid any nonlinear instabilities that may become apparent before the turbulent viscosity itself comes into play.

4.2. *Nonlinear Test*

In this second test, an incompressible, rotational vortex is combined with the uniform convection of the previous test-case in the same domain. The pressure and the density are

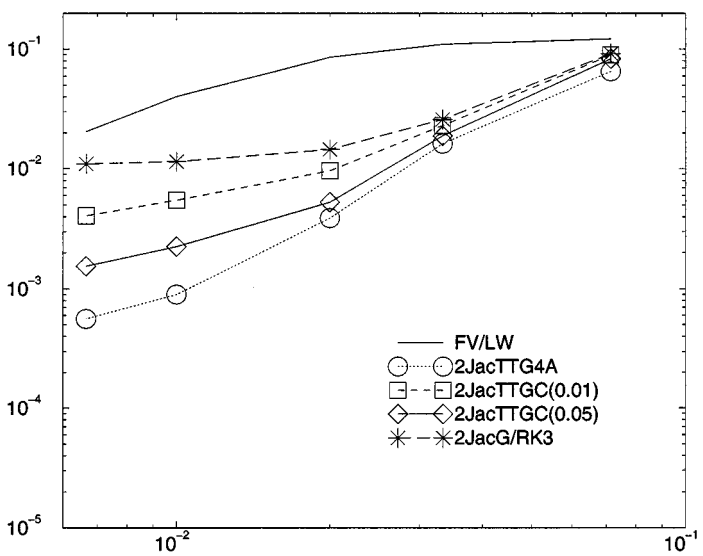

FIG. 18. L2 error versus mesh spacing on perturbed quadrilateral meshes for convection of a Gaussian pulse.

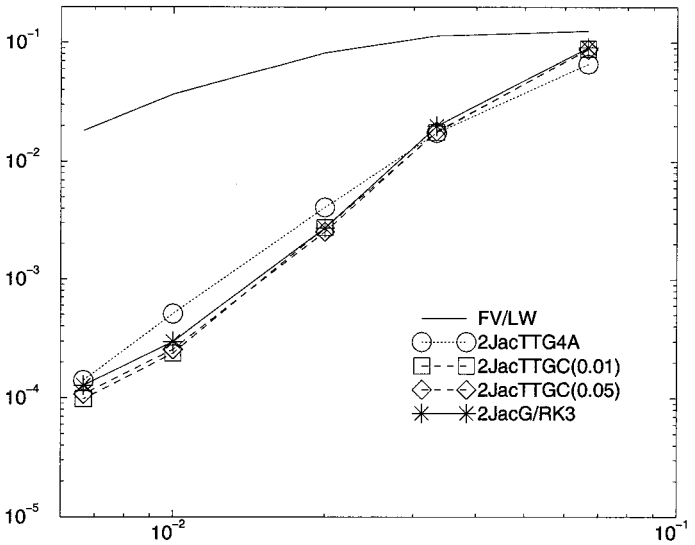

FIG. 19. L2 error versus mesh spacing on regular triangular meshes for convection of a Gaussian pulse.

uniform over the domain. The initial solution at $t = 0$ reads

$$\rho = \rho_0,$$
$$\Psi = \Psi_0 \exp(-((x - x_0)^2 + (y - y_0)^2)/\tau^2),$$
$$u_1 = u_0\left(1 - \frac{\partial \Psi}{\partial y}\right),$$
$$u_2 = u_0\left(1 + \frac{\partial \Psi}{\partial x}\right),$$

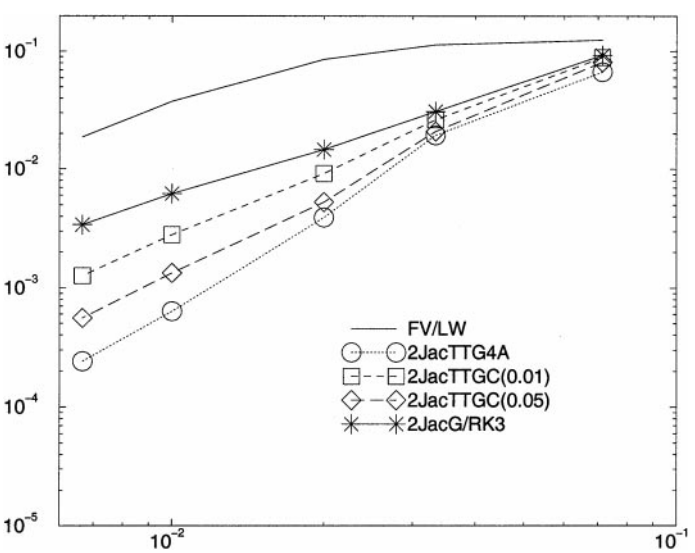

FIG. 20. L2 error versus mesh spacing on perturbed triangular meshes for convection of a Gaussian pulse.

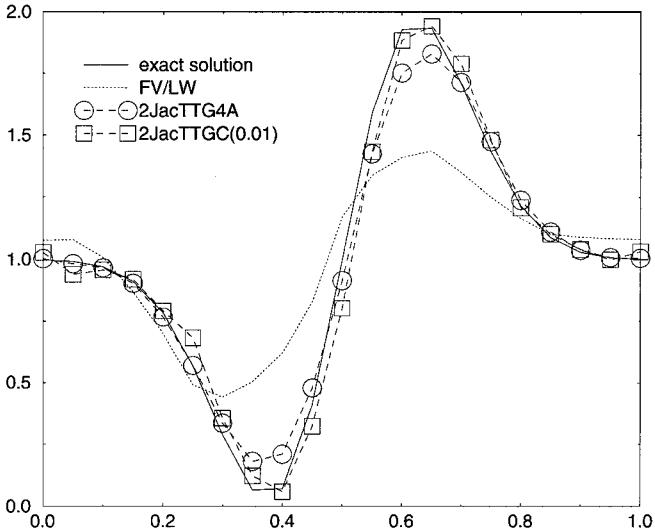

FIG. 21. Convection of a vortex on a perturbed 21^3 hexahedral mesh: $\Psi_0 = 0.2,\ \tau = 0.25/\sqrt{2}$.

$$u_3 = u_0,$$
$$p = p_0 - \rho_0 u_0^2 \frac{\Psi^2}{\tau^2},$$
$$E = \frac{p}{\rho(\gamma - 1)} + \frac{1}{2}\left(u_1^2 + u_2^2 + u_3^2\right),$$

with $\rho_0 = 1,\ u_0 = 1,\ \gamma = 1.4,\ p_0 = \rho_0/M_0^2\gamma,\ M_0 = 0.125,\ x_0 = y_0 = 0.5$.

This vortex should be convected without dissipation, and so we expect the solution at time $t = n$ (n integer) to correspond to the solution at time $t = 0$. However, the Jacobians of the Euler fluxes are no longer constant, since a rotation of the fluid is involved. Having locally linearised the Euler equations as in the previous section (i.e., using the product approximation for the fluxes and assuming that the Jacobians are constant within each cell), this test should demonstrate to what extent this assumption perturbs the solution.

Figure 21 shows the second velocity component along the line (0, 0.5, 0)-(1, 0.5, 0) at time $t = 1$ for $\Psi_0 = 0.2$ and $\tau = 0.25/\sqrt{2}$ in the case of a perturbed 21^3 hexahedral mesh. We see that TTGC(0.01) and TTG4A give comparable results, while the FV/LW scheme already shows an important dissipation error. Figure 22 shows the solution at $t = 1$ along the same cut but for a vortex with narrower cross-section (with approximately 2/3 the resolution of the previous vortex) and the same velocity amplitude ($\Psi_0 = 0.155$ and $\tau = 0.16/\sqrt{2}$). As this vortex contains higher Fourier modes, the dissipative error is more evident with TTG4A than with TTGC(0.01), while the FV/LW scheme has totally dispersed and dissipated the vortex. On this test, G/RK3 and TTGC(0.05) give results very similar to TTGC(0.01).

4.3. *Homogeneous Isotropic Turbulence (HIT) Decay without Viscous Terms*

This test is a basic test for unsteady LES computations. A synthetic three-dimensional turbulent flow (initialised with a Passot–Pouquet spectrum) is advanced in time on a periodic 21^3 hexahedral mesh. The CFL number is 0.7 and the mean and maximum Mach numbers

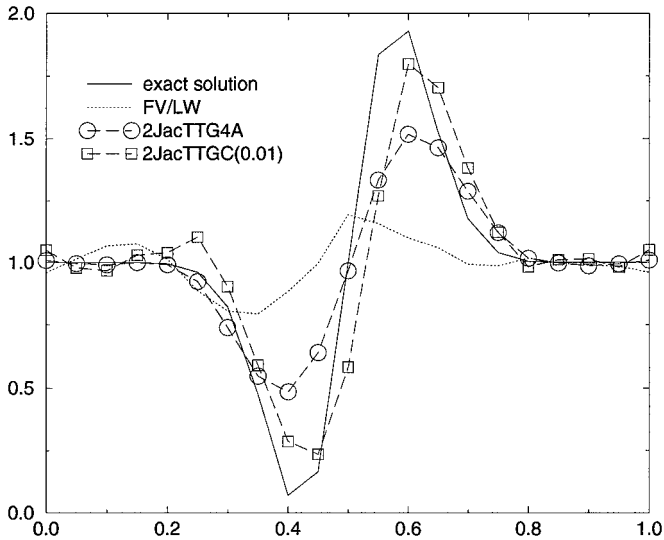

FIG. 22. Convection of a vortex on a perturbed 21^3 hexahedral mesh: $\Psi_0 = 0.155,\ \tau = 0.16/\sqrt{2}$.

at time $t = 0$ are 0.05 and 0.12, which are typical values for low Mach number tests. We define a convective CFL number $\mathrm{CFL}_{\mathrm{conv}} \approx \frac{\mathrm{Mach}}{1+\mathrm{Mach}}\mathrm{CFL}$, where $\mathrm{CFL} \approx (|u| + c)\Delta_t/\Delta_x$ is the Courant Friedrich number based on the velocity $|u| + c$ of the fastest acoustic waves in the simulation, and Δ_x is some length scale associated with the smallest element of the mesh. In this case the mean and maximum convective CFL numbers are approximately 0.033 and 0.075.

In this first test we do not make use of an LES model, nor do we consider the effect of laminar viscosity, so the calculation can be performed by solving the Euler equations. Consequently, we should see a progressive accumulation of energy and vorticity at high frequencies. In particular, the theory of turbulence [21] predicts a (monotonic) exponential growth of enstrophy as time increases, where enstrophy is defined as

$$\text{enstrophy} = \int_V (\nabla \times \mathbf{u})^2 \, dV.$$

Figures 23 to 27 show the time evolution of the mean enstrophy and kinetic energy for the various schemes described above (curves in solid line). We see that TTG4A dissipates enstrophy monotonically (after the initial growth), while TTGC and G/RK3 lead to the exponential growth predicted by the theory. FV/LW also predicts the growth but with an important decrease of enstrophy prior to it.

This test already indicates that TTG4A, and to a lesser extent FV/LW and TTGC(0.05), may be too dissipative to carry out LES calculations, as their intrinsic dissipation already acts as an ad hoc LES viscosity model. This behaviour is in line with the Fourier analysis of Subsection 2.3, which shows that the TTGC scheme has substantially less high frequency dissipation for low CFL numbers. Since turbulent motion is convected numerically at the convective CFL number defined above, we may expect such behaviour for all low Mach number cases (say $\mathrm{Mach} < 0.3$). It is the acoustic waves that are convected at the true CFL number, and it is only high frequency acoustic waves that will be adversely effected by large dissipative and dispersive errors, although these are often less important in LES

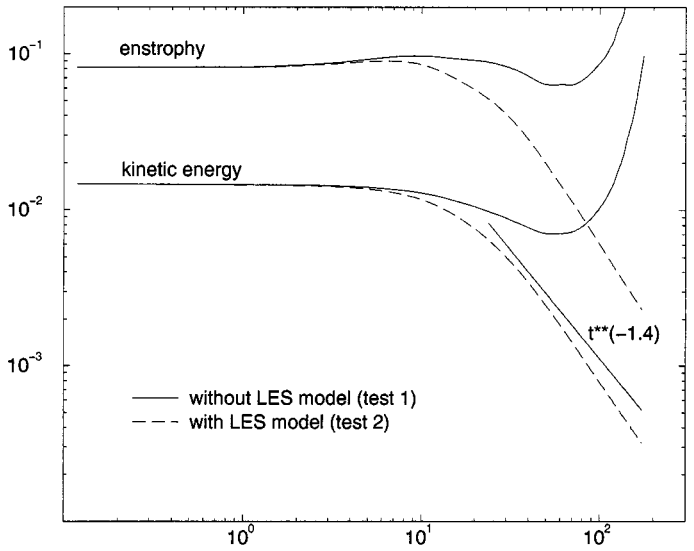

FIG. 23. HIT test for FV/LW scheme.

computations. Even then the time step is limited by the smallest elements of the mesh and so acoustic waves are effectively convected at low CFL numbers over the majority of an unstructured mesh for many practical applications.

4.4. *Homogeneous Isotropic Turbulence Decay with LES Viscosity Model*

Starting from the same solution and the same mesh as above, we now add the laminar and turbulent viscosity terms. The turbulent eddy viscosity model employed is the filtered Smagorinsky model [22]. Since we are using a (bi-)linear finite-element approximation for which viscous terms can not be approximated to third-order accuracy [23], we make use of a standard second-order approximation for these terms (using one-point quadrature

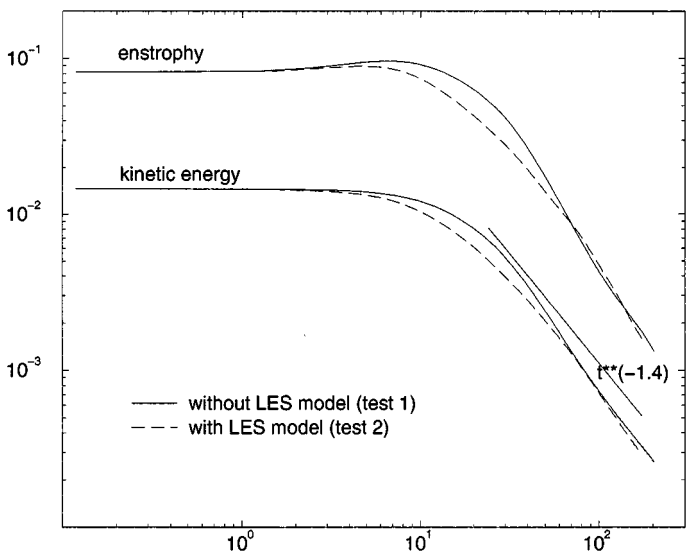

FIG. 24. HIT test for 2JacTTG4A scheme.

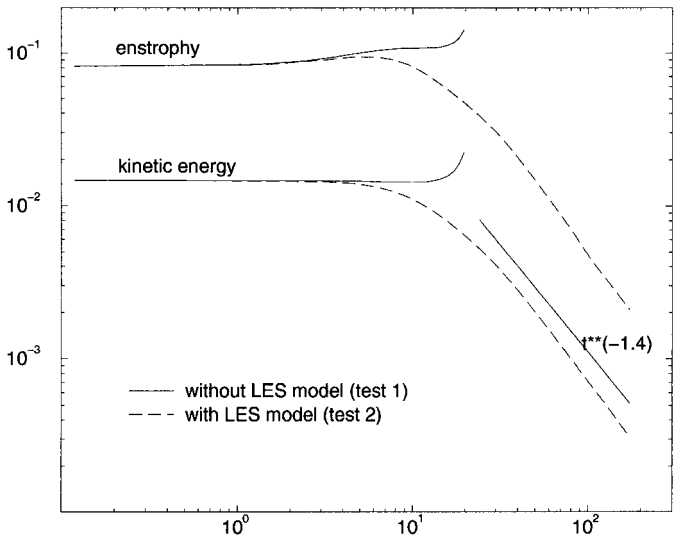

FIG. 25. HIT test for 2JacTTGC(0.01) scheme.

for simplicity), although we retain third-order for convective terms. This approximation is justified in the context of LES calculations where important simplifications have already been used to derive the LES model itself.

In Figs. 23 to 27 we present the evolution in time of mean enstrophy and kinetic energy for this second test (dashed lines). As the initial solution contains no energy at the highest frequencies, vorticity and energy are fed into these modes through the energy cascade mechanism, which explains the initial growth in enstrophy from time $t = 0$ to $t = 6$. As vorticity at high frequencies grows, turbulent viscous terms start to become effective in dissipating these quantities. We note that theoretical [13] and experimental results predict a $t^{-1.4}$ law for the asymptotic decay in kinetic energy.

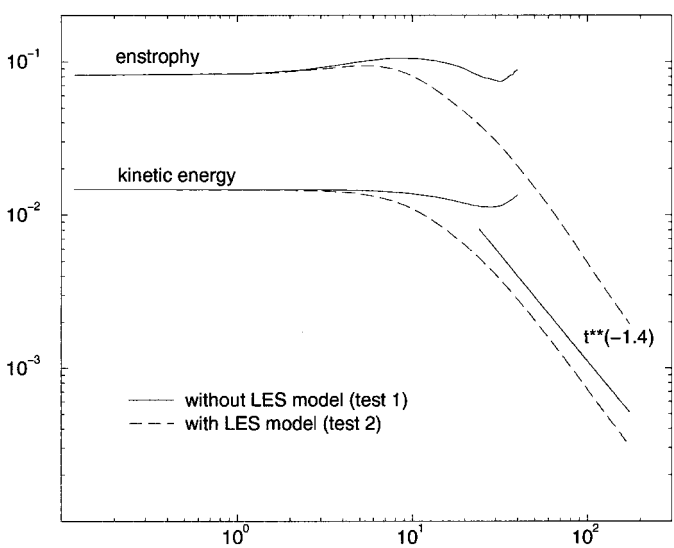

FIG. 26. HIT test for 2JacTTGC(0.05) scheme.

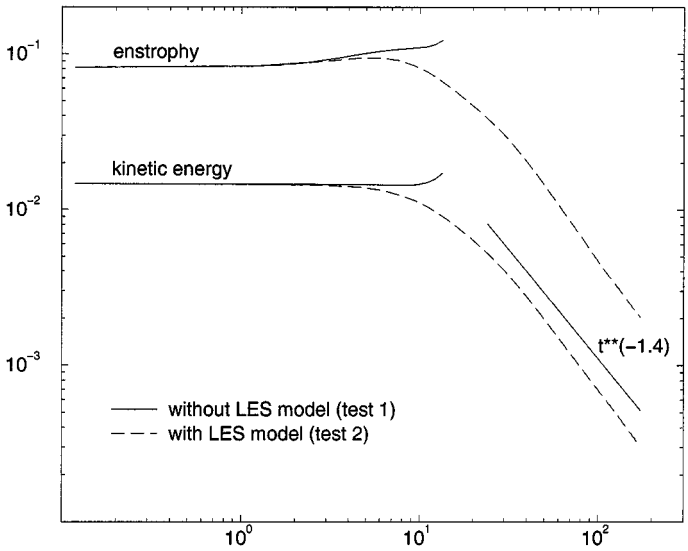

FIG. 27. HIT test for 2JacG/RK3 scheme.

By comparing the evolution of mean enstrophy and kinetic energy with and without LES viscous terms it is evident that the dissipation rate of kinetic energy is not entirely dictated by the LES viscosity model, as it would be ideally. Instead, it is dependent on the numerical dissipation that is inherent to the convective scheme. For G/RK3, TTGC(0.01), and TTGC(0.05), which show good agreement with theory, it can be concluded that the LES model is responsible for most of dissipation of energy, and not numerical viscosity. Meanwhile, the results for TTG4A show nearly identical evolutions of enstrophy and kinetic energy for both the viscous and inviscid tests, indicating that the LES model has a marginal effect compared to numerical dissipation. This is confirmed by the evolution of the mean turbulent viscosity in Fig. 28: the mean level for TTG4A is significantly smaller than for

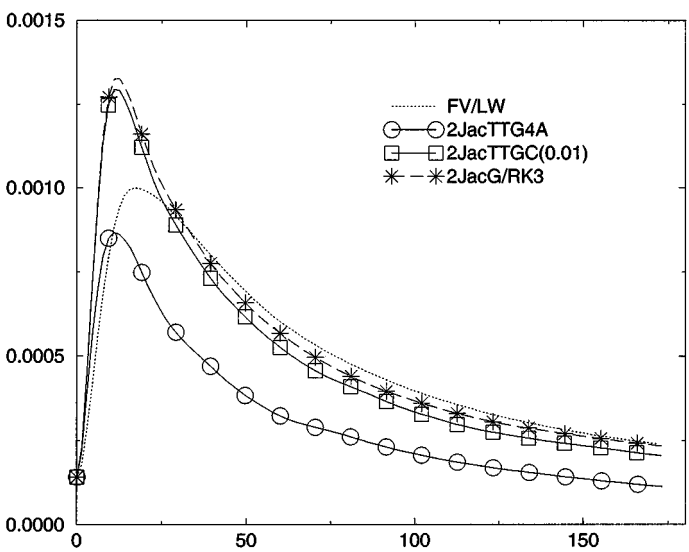

FIG. 28. Time evolution of mean turbulent viscosity for HIT test with turbulent viscosity model.

TABLE II
Total CPU Time per Iteration on a 21^3 Periodic Mesh

Scheme	Hexahedra CPU time (in s)	Hexahedra CPU time/LW time	Tetrahedra CPU time (in s)	Tetrahedra CPU time/LW time
FV/LW	0.82	1.	1.57	1.
2JacTTG4A	2.23	2.7	3.00	1.9
2JacTTGC	2.04	2.5	3.02	1.9
4JacTTGC	2.36	2.9	3.5	2.2
nJacTTGC	$1.73+0.157n$	$2.1+0.19n$	$2.55+0.237n$	$1.6+0.15n$
2JacG/RK3	2.44	3.0	4.00	2.5

other schemes. The FV/LW scheme shows intermediate behaviour between these two trends. TTGC(0.01), TTGC(0.05), and G/RK3 give approximatively a $t^{-1.5}$ law for the kinetic energy decay while TTG4A and FV/LW give powers of -1.55 and -1.63, respectively, which again indicates excessive dissipation.

This second test confirms that G/RK3 and TTGC(0.01) behave much better than FV/LW and that TTG4A is definitely too dissipative for LES applications. The difference observed between TTGC(0.01) and TTGC(0.05) indicates that as the parameter γ is increased, the scheme becomes more dissipative at high frequencies and it too becomes less suitable for LES.

5. COMPUTATIONAL COST

In order to give an approximate idea of computational cost, we measure the total CPU time per iteration for the different schemes studied on the 21^3 periodic mesh. Note that all of the schemes were developed within the same computational code, and so all common components are shared. By the same token, no optimisations that may be *particular* to a given scheme have been performed, although we are reasonably confident that in most cases the figures give a realistic assessment of relative cost.

Table II shows CPU times for hexahedral and tetrahedral elements. The third and fifth columns give CPU times normalised by the cost of the basic FV/LW scheme described in [15]. For both element types we see that the TG schemes (with 2 Jacobi iterations) are 1.9 to 3 times slower than FV/LW, which indicates that the improvement brought by these schemes can be obtained at a very reasonable cost for practical calculations. Tetrahedral calculations are found to be 1.3 (for 2JacTTG4A) to 1.9 (for FV/LW) slower than the calculation on hexahedra for the same number of unknowns: this is explained by the increased number of cells treated with tetrahedra (40000 versus 8000) since each hexahedron is replaced by 5 tetrahedra for the regular grids considered here. TTGC can be seen to be substantially faster than G/RK3 (there is between 20 and 32% of overhead for G/RK3), while TTGC and TTG4A have comparable CPU times. Since TTGC(0.01) and G/RK3 give similar solutions on simple test cases, TTGC will be preferred on practical calculations for its lower cost, as well as offering increased robustness on irregular complex meshes.

6. CONCLUSION AND FUTURE WORK

In this article the construction of various Taylor–Galerkin (TG) finite-element schemes has been described and a new TG scheme, TTGC, has been proposed. Our goal was to

develop practical schemes for LES, and so methods that are particularly suitable for implementation within an unstructured parallel solver have been derived. This involved approximation of the integrals that occur in the discrete space-time equations in a manner that is substantially cheaper than well-known quadrature techniques, while preserving discrete conservation. The resulting schemes recover the exact finite-element formulation on regular elements, and tests carried out on perturbed elements indicate that, although approximate, the method still gives good results.

Using these formulations, the TG schemes considered have been demonstrated on three-dimensional linear and nonlinear advection test-cases and were seen to give substantially better results than the second-order Lax–Wendroff and centred three-step Runge–Kutta schemes. Tests were also performed for all basic element types (namely quadrilaterals, triangles, tetrahedra, prisms, pyramids, and hexahedra) and indicate similar properties for all of these, as well as for hybrid meshes. Mesh refinement studies indicate that the TG schemes presented do give third-order accurate solutions for convective terms on regular meshes, although decreased orders are evident on perturbed meshes, especially for the less dissipative of them (G/RK3 and TTGC(0.01)). A detailed study of this phenomenon has not been carried out, as this is beyond the scope of the present paper—our aim here was to describe a practical method with minimal computational overhead compared with existing low-order schemes.

For the LES applications that are of primary interest to us, we have established that the ETG and TTG4A schemes are too dissipative, despite the fact that they offer improved phase accuracy over standard second-order schemes. Our new TG scheme, TTGC, essentially retains the same structure as standard TG schemes although it results in lower dissipative errors at high frequencies, comparable to those given by the three-step Runge–Kutta–Galerkin scheme (G/RK3). In essence, the new approximation offers a compromise between existing TG schemes and G/RK3 and, at least for the problems we are interested in, strikes a balance between the dissipation that is needed to maintain nonlinear stability on irregular meshes, the requirements of LES, and the need to minimize computational costs.

Future development will be driven by activities on LES calculations of turbulent combustion in complex geometries, which will be reported elsewhere.

APPENDIX: CONSERVATION PROPERTY OF TG SCHEMES

We present here the practical definition of conservation adopted in our work and the proof that our schemes fulfill this criterion. The definition of conservation involves consistently approximating the integral form of the PDE over the domain

$$\int_t^{t+\Delta t} \int_\Omega u_t \, dV \, dt = - \int_t^{t+\Delta t} \int_{\partial\Omega} F \, dS \, dt. \tag{54}$$

For our finite-element discretisation, we shall demand that

$$\int_\Omega \frac{U^{n+1} - U^n}{\Delta t} dV = - \overline{\int_{\partial\Omega} F \, dS}, \tag{55}$$

where $\overline{\int_{\partial\Omega} F \, dS}$ is some (as yet undefined) approximation of the global flux integral.

For the schemes of interest,

$$\int_\Omega \frac{U^{n+1}-U^n}{\Delta t}\,dV = \int_\Omega \sum_i \Phi_i \left(\frac{U_i^{n+1}-U_i^n}{\Delta t}\right) dV = \sum_i V_i R_i^{n+1}, \tag{56}$$

with V_i the mass-lumped coefficient of node i,

$$V_i = \int_\Omega \Phi_i\,dV = \sum_j M_{ij}. \tag{57}$$

We note that

$$\sum_j V_j R_j^{n+1} = \sum_i \sum_j M_{ij} R_j^{n+1} = \sum_i \int_\Omega R^{n+1}\Phi_i\,dV = \sum_i H_i^n = \sum_c \sum_{i\in\Omega_c} H_i^n\big|_c, \tag{58}$$

where $H_i^n|_c$ is the restriction to cell c of the RHS operator of the TG scheme considered. The condition (55) then reads

$$\sum_c \left(\sum_{i\in\Omega_c} H_i^n\big|_c\right) = \overline{\int_{\partial\Omega} F\,dS}, \tag{59}$$

and since the mesh is arbitrary, and assuming our approximate surface integrals cancel out across internal faces,

$$\sum_{i\in\Omega_c} H_i^n\big|_c = \overline{\int_{\partial\Omega_c} F\,dS}. \tag{60}$$

The RHS operator H_i^n is a linear combination of the operators L and LL. A sufficient condition on L and LL for Eqs. (60) and (59) to be satisfied is then

$$\sum_{i\in\Omega_c} L_i(U^n)|_c = \overline{\int_{\partial\Omega_c} F\,dS}, \tag{61}$$

$$\sum_{i\in\Omega_c} LL_i(U^n)|_c = 0. \tag{62}$$

In the linear case, it is straightforward to show that by summing Eq. (43) over the nodes of the mesh gives Eq. (61), where

$$\overline{\int_{\partial\Omega_c} F\,dS} = V_c(\nabla\cdot F)_c = V_c(\nabla\cdot F)_{FV}. \tag{63}$$

In the bi/tri-linear case, summing Eq. (52) over the nodes of the element gives

$$\sum_{i\in\Omega_c} L_i(U^n)|_c = V_c(\nabla\cdot F)_{FV} + \sum_j F_j\,\overline{T}\left(\sum_i \tilde{\Theta}_{ij}\right).$$

The first term on the right-hand side is the finite-volume divergence term obtained in the linear case. Summing Eq. (51) over the nodes of the element proves that the second term in parentheses cancels out,

$$\begin{aligned}\sum_i \tilde{\Theta}_{ij} &= \int_{\tilde{\Omega}_c}\left(\sum_i \Phi_i\right)\left(\nabla\Phi_j - \frac{1}{I_c}\int_{\tilde{\Omega}_c}\nabla\Phi_j\,dV\right)dV\\ &= \int_{\tilde{\Omega}_c}\nabla\Phi_j\,dV - \frac{1}{I_c}\left(\int_{\tilde{\Omega}_c} 1\,dV\right)\left(\int_{\tilde{\Omega}_c}\nabla\Phi_j\,dV\right).\end{aligned}$$

As we arbitrarily chose $\int_{\tilde{\Omega}_c} = I_c$, the right-hand side is zero and Eq. (61) is satisfied.

Finally, equality (62) is proven by using definition (36) and (38) of LL,

$$\sum_{i\in\Omega_c} LL_i(U^n)|_c = (A,\, B,\, C)\left(\sum_j F_j\left(\int_{\Omega_c}\nabla\Phi_j\left(\sum_i \nabla\Phi_i\right)^T\right)\right).$$

As $\sum_i \nabla\Phi_i = 0$, (62) is satisfied, and the scheme is conservative for bi/tri-linear elements.

ACKNOWLEDGMENTS

This work was carried out at Oxford University Computing Laboratory and was supported by CERFACS, AEROSPATIALE MATRA MISSILES, and the Smith Institute.

REFERENCES

1. A. G. Kravchenko and P. Moin, On the effect of numerical errors in large eddy simulations of turbulent flows, *J. Comput. Phys.* **131**, 310 (1997).
2. H. Choi, P. Moin, and J. Kim, Direct numerical simulation of turbulent flow over riblets, *J. Fluid Mech.* **255**, 503 (1993).
3. J. Kim, P. Moin, and R. Moser, Turbulence statistics in fully-developped channel flow at low Reynolds number, *J. Fluid Mech.* **177**, 133 (1987).
4. S. Lele, Compact finite difference schemes with spectral like resolution, *J. Comput. Phys.* **103**, 16 (1992).
5. C. Hu and C.-W. Shu, *Weighted Essentially Non-oscillatory Schemes on Triangular Meshes*, Technical Report NASA/CR-98-208459, ICASE Report No.98-32, November 1998.
6. M. B. Giles and W. T. Thompkins, Propagation and stability of wavelike solutions of finite difference equations with variable coefficients, *J. Comput. Phys.* **58**(3), 349 (1985).
7. A. Jameson, W. Schmidt, and E. Turkel, *Numerical Solutions of the Euler Equations by Finite Volume Methods using Runge–Kutta Time-Stepping Schemes*, AIAA paper 81-1259, June 1981.
8. J. Donea and L. Quartapelle, An introduction to finite element methods for transient advection problems, *Comput. Methods Appl. Mech. Eng.* **95**, 169 (1992).
9. J. Donea, A Taylor–Galerkin method for convective transport problems, *Int. J. Numer. Methods Eng.* **20**, 101 (1984).
10. L. Quartapelle and V. Selmin, High-order Taylor–Galerkin methods for non-linear multidimensional problems, *Finite Elements Fluids*, 1375 (1993).
11. A. Safjan and J. T. Oden, High-order Taylor–Galerkin and adaptive h-p methods for second-order hyperbolic systems: Application to elastodynamics, *Comput. Methods Appl. Mech. Eng.* **103**, 187 (1993).
12. A. Safjan and J. T. Oden, High-order Taylor–Galerkin methods for linear hyperbolic systems, *J. Comput. Phys.* **120**, 206 (1995).
13. M. Lesieur and O. Metais, New trends in large-eddy simulations of turbulence, *Ann. Rev. Fluid. Mech.* **28**, 45 (1996).
14. Y. Morinishi, T. S. Lund, O. V. Vasilyev, and P. Moin, Fully conservative higher order finite difference schemes for incompressible flow, *J. Comput. Phys.* **143**(1), 90 (1998).
15. T. Schönfeld, C. Angelberger, JP. Legier, and S. Ducruix, *Numerical Simulation of Compressible Reactive Flows on Unstructured Grids*, AIAA paper 99-0414, January 1999.
16. J. Donea, L. Quartapelle, and V. Selmin, An analysis of time discretization in the finite element solution of hyperbolic problems, *J. Comput. Phys.* **70**, 463 (1987).
17. V. Selmin, *Third Order Finite Element Schemes for the Solution of Hyperbolic Problems*, INRIA Report, 707, 1987.

18. A. J. Wathen, On relaxation of Jacobi iteration for consistent and generalized matrices, *Appl. Numer. Methods* **7**, 93 (1991).
19. A. J. Wathen, Realistic eigenvalue bounds for the Galerkin mass matrix, *IMA J. Numer. Anal.* **7**, 449 (1987).
20. T. Schönfeld and M. Rudgyard, Steady and unsteady flow simulations using the hybrid flow solver AVBP, *AIAA J.* **37**(11), 1378 (1999).
21. M. Lesieur, Turbulence in fluids, in *Fluid Mechanics and Its Applications* (Kluwer Academic, Dordrecht, 1990), Vol. 1.
22. F. Ducros, F. Nicoud, and T. Schönfeld, Large-eddy simulation of compressible flows on hybrid meshes, in *Eleventh Symposium on Turbulent Shear Flows, Grenoble, France, 1997*.
23. J. Donea, S. Giuliani, H. Laval, and L. Quartapelle, Time-accurate solution of advection-diffusion problems by finite elements, *Comput. Methods Appl. Mech. Eng.* **45**, 123 (1984).